IEEE Access
Multidisciplinary | Rapid Review | Open Access Journal

Received 22 January 2025, accepted 11 February 2025, date of publication 26 February 2025, date of current version 11 March 2025.

Digital Object Identifier 10.1109/ACCESS.2025.3545917

APPLIED RESEARCH

Design of a Horizontal and Vertical Polarized Slotted Waveguide Antenna Array for an Airborne Ka-Band Polarimetric Interferometric SAR System

ALICJA SCHREIBER, MARKUS LIMBACH, AND BERND GABLER, (Member, IEEE)
German Aerospace Center, Microwave and Radar Institute, 82234 Oberpfaffenhofen, Germany
Corresponding author: Alicja Schreiber (alicja.schreiber@dlr.de)

ABSTRACT This paper presents the design of a fully polarimetric low-profile antenna array intended for use in a side-looking airborne synthetic aperture radar (SAR) sensor operating at Ka-band. The proposed antenna provides maximum gain of up to 23 dB, a low side lobe level and high cross-polarization suppression values exceeding 38 dB. Furthermore, the proposed antenna demonstrates robust behavior and stable electrical performance in a variety of environmental conditions encountered during the measurement campaigns. The antenna system was designed using slotted waveguide technology, comprising separate antenna arrays for each polarization, which were mounted side by side on the aircraft platform. An appropriate design was developed based on theoretical analysis, considering the specifications of the electrical and mechanical systems. The horizontally polarized antenna consists of four subarrays, each comprising 22 transverse slots cut into the narrow waveguide wall. The alternately placed iris pairs enable radiation. The antenna with vertically polarized radiation is realized through the implementation of four subarrays, comprising 18 longitudinal slots, situated within the broad waveguide wall. Appropriate feeding networks with unbalanced amplitude distributions were designed to feed both arrays. For the horizontally polarized antenna, a conventional H-plane T-junction power divider and a Bethe-hole directional waveguide coupler were used. In contrast, a two-stage H-plane T-junction with a non-uniform amplitude taper was applied for vertical polarization. The proposed design was validated by compact test range measurements, which demonstrated a very good agreement with the simulation results.

INDEX TERMS Airborne SAR system, polarimetric interferometry, Ka-band antenna array, dual-polarized slotted waveguide antenna (SWA).

I. INTRODUCTION

In recent years, airborne SAR systems have played an important role in remote sensing applications [1]. This is due to the specific advantages inherent to radar-based assemblies, including all-weather readiness and a day-and-night operational capability. A significant advantage of airborne systems is the capacity to validate novel technologies and evaluate their suitability for future satellite missions in advance. The utilization of such a system enables the testing of both hardware and processing software, in addition to data retrieval algorithms, which constitutes a pivotal stage in the development of satellite systems. Moreover, an airborne sensor offers a versatile, adaptable, and accessible platform for remote sensing operations, thereby facilitating the optimization of instrument design.

There are many airborne SAR systems operated all over the world for both civilian and military applications, that differ from system parameters and intended purpose [2], [3], [4], [5], [6], [7], [8]. The Microwaves and Radar Institute at

The associate editor coordinating the review of this manuscript and approving it for publication was Pavlos I. Lazaridis.

the German Aerospace Center (DLR) in Oberpfaffenhofen operates such a sensor (F-SAR) and constantly improves its capabilities using new technologies and methods [9]. It is flown onboard an aircraft Dornier Do-228 and currently consists of eight fully polarimetric antennas operating in five different frequency bands, spanning from P-band up to X-band [10], [11], [12], [13]. One noteworthy property of the F-SAR system is its ability to operate up to four frequencies simultaneously, allowing for the acquisition of various data regarding the overflown region. To further enhance this capability, the development of an additional sensor operating at Ka-band was initiated.

Systems operating in this frequency band have attracted considerable attention in recent years, largely due to their compact size and lightweight design. They have also been the focus of promising research areas such as ice monitoring and water surface measurements, which have provided valuable insights into climate change observations. Consequently, there are a number of existing airborne Ka-band SAR systems that were designed for different purposes and thus individually adjusted to meet the required performance specifications. For example, the AirSWOT radar interferometer [14], designed by NASA, is an experimental airborne Ka-band instrument that is used to validate the forthcoming NASA Surface Water and Ocean Topography (SWOT) satellite mission. The system operates in cross-track interferometry mode and is capable of functioning in multiple polarization configurations, enabling the measurement and analysis of diverse backscattering properties of water surfaces. In contrast, the PAMIR-Ka SAR demonstrator [8] is a single-polarized airborne sensor currently under development at Fraunhofer FHR. It features a quasi-monostatic antenna arrangement and is primarily utilized to examine relevant SAR imaging aspects in Ka-band. The wide bandwidth enables the processing of SAR images with high azimuth resolution. MetaSensing has developed a single-pass interferometry airborne SAR system in Ka-band, known as KaSAR [2]. The system is composed of dual-polarized slotted waveguide antennas, which are mounted on the aircraft with adjustable baselines. This sensor operates in frequency-modulated continuous wave mode (FMCW), which is better suited for applications requiring high precision at short to medium range. In contrast, a pulsed radar system used in F-SAR is more suitable for long-range applications. The Ka-band imaging radar DRIVE, developed by ONERA, is also operational in frequency-modulated continuous wave (FMCW) mode and operates as a single-polarized nadir-looking radar dedicated to imaging non-smooth areas [15].

The Ka-band sensor, which is the subject of this article, operates in a single-pass interferometry configuration at a center frequency of 35.5 GHz. It represents a part of the Ka-PolInSAR system, comprising two fully polarimetric transmit and up to four fully polarimetric receive antennas, which are mounted on a carbon fiber structure located underneath the fuselage of the Dornier Do-228 aircraft. The utilization of a dual-polarized system allows for the acquisition of diverse information regarding the structure of the imaged surface, as the scattering characteristics are dependent on the polarization used. The innovative Ka-band antenna is designed to operate in a side-looking mode with mechanical beam steering at an incident angle of 45°. The antenna carrier permits the antennas to be mounted in a variety of positions, thereby facilitating the attainment of diverse baselines for interferometry modes. This enables the sensor to generate a number of configurations for a variety of scenarios and applications. In general, antennas mounted on an aircraft platform are constrained by the limited space available. The antenna carrier for Ka-Band operations at the Dornier Do-228 is situated within the installation area of the F-SAR P-Band antenna, thereby ensuring that a sufficient volume for antenna installation is provided. Furthermore, the very short wavelength enables the reduction of antenna and network dimensions. The objective of the new system, operated in the Ka-band frequency, is to gain information about the structure of the upper snow cover, as well as to access biophysical parameters such as snow-water equivalent, snow cover or firn lines in high mountain areas and glaciers. The challenge of designing a fully polarimetric antenna system with high-power capability and extreme beam stability over the required frequency bandwidth, that induces low side lobe- and cross-polarization levels as well as airworthiness requirements are some of the innovative aspects of this work.

This article is structured as follows: in section II, the mechanical and electrical requirements for airborne SAR antennas are specified and their significance in the SAR image quality are explained. Later, in section III the theoretical basics of the slotted waveguide antenna technology are presented and the antenna arrangement on the airplane is shown. Consequently, the design and development of the antenna array with detailed development description showing step by step the single antenna element design, the antenna array configuration and the appropriate network for both horizontal and vertical polarizations. Next, in section IV the measurement results for both antennas are shown. Subsequently, the comparison with other works about the Ka-band antennas is presented in section V. Finally, the outcomes of this study are discussed in section VI.

II. ANTENNA SYSTEM REQUIREMENTS

As the Ka-band antennas used for the extension of the F-SAR sensor, serve as a part of a side-looking airborne radar system, a range of different mechanical and electrical requirements must be fulfilled [1], [16]. A detailed description can be found in following subchapters.

A. ELECTRICAL REQUIREMENTS

Fig. 1 illustrates a typical SAR geometry, where the platform moves in the azimuth or flight direction, whereas the range or elevation is the direction perpendicular to the radar flight path, looking to the ground beneath the flight path. For DLR's

airborne SAR system this is typically a right looking configuration, focusing on an angular range of approximately 20° to 65° off-nadir [9] and causes in the main lobe pointing at about 45°.

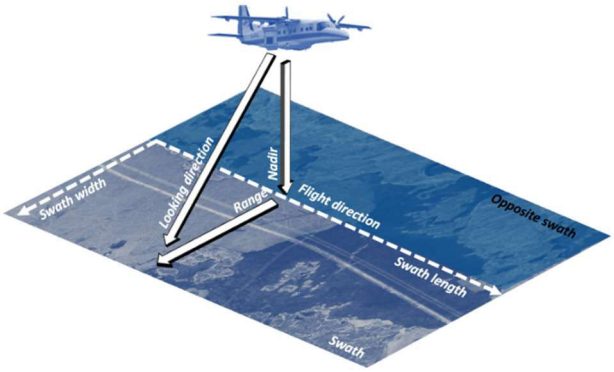

FIGURE 1. The typical side-looking airborne SAR acquisition.

This arrangement results in some general demands for antenna design. For reasons of unambiguity, the area opposite the nadir track must be suppressed. In particular, the nadir direction is of critical importance due to the perpendicular reflection of the radar signal on the ground. In conclusion, the elevation pattern must suppress the nadir signal and the opposite swath area by at least 25 dB, one way, while simultaneously supporting the swath, area of interest, with an equally shaped main beam pattern. It is necessary to compensate for the longer propagation path length in the far range with slightly higher gain values in comparison to the near range. With regard to both azimuth and elevation, the level of the side lobes should be less than 18 dB, at least. Not all conditions can be discussed in detail here. The values for the aforementioned parameters were derived from SAR processing and bases on Nyquist criteria as well as sufficient and evenly echo strength along range direction. Thus, fulfilling these requirements guarantees that objects can be clearly categorized spatially. Most interface parameters are driven by the radar hardware like frequency of operation and bandwidth of the system which are given by the high power TWTA (traveling wave tube), which was specially designed and manufactured for this airborne environment. In systems operating at higher frequencies, where free space losses are increased, it is crucial to design maximum-gain antennas capable of withstanding high transmit power, as used in this application. In the absence of this, the signal-to-noise ratio (SNR) will be insufficient for the processing of a high-quality SAR image from the received data. In order to satisfy the requirement of gain at least 20 dBi, the antenna must possess a larger aperture size comprising a greater number of elements. This, in turn, allows for more extensive shaping of the main lobe, particularly in relation to the side lobes. However, in order to ensure optimal system performance and image quality in terms of resolution, it is essential to consider the antenna half-power beam width in azimuth in relation to critical parameters such as platform velocity and the system pulse repetition frequency (PRF).

TABLE 1. The required antenna array parameters.

Variable	Parameter	Value
f_0 [GHz]	frequency of operation	35.5
BW [GHz]	bandwidth	0.5
P_T [kW]	Transmit peak power	2.5
PRF [Hz]	pulse repetition frequency	6000
SLL [dB]	side lobe level (SLL)	> 18
θ_{El} [°]	half-power beam width in elevation	21
θ_{Az} [°]	half-power beam width in azimuth	5
G [dBi]	gain	> 20
-	opposite swath suppression	> 25
-	nadir suppression	> 25
-	side-looking SAR acquisition	45° beam steering
-	cross-polarization suppression	> 25
-	polarization	linear vertical/horizontal

Accordingly, the system specification is set to a 5° half-power beam width in azimuth and approximately 21° in elevation and leads as a tradeoff between sufficient SNR to produce unambiguous, non-noisy SAR image and obtaining the desired swath width. The required antenna parameters are collated in Table 1.

B. MECHANICAL REQUIREMENTS

The use of the aircraft as a mounting platform leads to additional mechanical requirements. First of all, the total weight of the radar system has to be minimized as much as possible, since additional weight is related to reduces endurance. The fact that the antenna system consists not only of the antennas themselves but also of additional support structures and aerodynamic parts increases the need of low weight components. Furthermore, aerodynamic requirements are integrated into the antenna system design, which also considers icing conditions, induced drag, turbulence and a broader range of mechanical vibrations. Consequently, low-profile antennas are the optimal choice for aircraft installation, which in turn restricts the range of antenna types that can be selected. It is essential that materials and design take into account the various mechanical forces acting on the aircraft installation, in order to prevent the antenna from fracturing as a result of excessive forces and fatigue. The environmental conditions of the airborne campaigns are varying during the flight and are depending on the type of mission. In this way, the antenna must be able to deliver the same electrical performance under different outdoor conditions. Thus, there must be no corrosion or deformation due to temperature differences or air humidity.

The installation area for the Ka-band system is determined and not free to choose. The installation framework is part of the requirements and is supposed to be in front of the aircraft, underneath the fuselage, which is an additional challenge. In order to protect sensitive parts of the antenna from stone chipping or contamination during take-off and landing, a suitable radome has to be apply.

III. ANTENNA ARRAY DESIGN

A. TECHNOLOGY

The antenna arrays presented in this article are designed using slotted waveguide antenna technology (SWA) composed with the air-filled metallic waveguides [17], [18], [19]. This technique impresses with its high performance, agile aperture distribution control, low losses, high power handling capability and robust behavior. If no dielectric material is used, it also enables the maximum possible gain. Furthermore, this antenna type meets the requirement for a low-profile construction. The substrate integrated waveguide (SIW) technology frequently referenced in the extant literature [20], [21], [22], [23], [24], [25], [26] is not applicable to this particular application. Despite its apparent advantages, including a compact design, low weight and low cost, the technology generates dielectric losses that compromise the system, particularly at higher frequencies. Since the system must be capable of accommodating high transmission power also renders this technology inapplicable. This is due to the fact that even in a low-loss SIW structure, high power levels result in thermal losses that must be effectively dissipated to prevent overheating. Consequently, this may result in the degradation of the material and alterations to the electrical properties. The potential limitations associated with the dimensions of the feeding network made by a metal air-filled waveguides are mitigated by the installation framework, which provides supplementary space behind the antenna installation base plate.

SWAs are waveguides with slots cut into either a broad or a narrow wall. The slot position is set in such a way, that thereby the current flow interruption is achieved or an additional structure is needed to reach this process. Thus, the electric field occurs between opposite sides of the slot and couples out into the free space. The slot impedance has to be adapted to the waveguide one, which ensures that maximum power is coupled into the slot. In order to emit this power, it must be guaranteed that it is not lost as reactive power loss due to the electromagnetic field redistribution. This, in turn, is achieved by operating the slot in resonance at a certain length.

There are several possibilities to locate the slot on the waveguide, which can be cut longitudinal, transversal or edge in the narrow or broad waveguide wall. The slots are usually distributed along the waveguide forming an array. Therefore, to obtain the radiation, the slots should satisfy two conditions. Firstly, the distance between successive slots should be close to the half-guided wavelength, in order to achieve a grating lobe free far-field pattern. Secondly, they should generate an in-phase signal between two consecutive slots to interfere constructively in far-field. The polarization of the electromagnetic wave generated by the slot depends on its position on the waveguide and the alignment of the antenna on the aircraft, which may be either horizontal or vertical. As mentioned in previous section, the Ka-PolInSAR requirement for a narrower beam in flight direction and wider one in range purports in fact the antenna arrangement on the airplane. Th antenna is mounted with its long side parallel to the flight direction, where the waveguide with several slots act as a subarray in this plane and thus fulfil the requirement on the narrow beam. In order to generate vertically polarized electromagnetic wave, SWA consist of longitudinal slots cut into a broad waveguide wall. For the horizontally polarized antenna, the slots are typically cut inclined into the narrow wall of the waveguide [27], which is from the manufacturing point of view easier to realize. Nevertheless, the cross-polarization level attained in this configuration is relatively high, which is an unfavorable outcome for this particular application. Consequently, to create horizontally polarized signals the narrow waveguide wall is cut with the transversal slots. This slot position does not cause current interruption, since the slots run parallel to the current flow. To force the radiation, an additional structure inside the waveguide is needed to provide this process. The exact implementation in this regard is explained in the section B.

On the beginning of this project, the antenna array was originally conceived as consisting of alternately located vertically and horizontally polarized individual subarray elements in terms of creating a preferable small phase center shift between both polarizations. Accordingly, referred to the grating lobe free far-field pattern for the antenna, it is necessary to position the elements of the same polarization at a distance of less than the free space wavelength calculated for the center frequency, which is equal to λ_0 =8.45 mm. This approach cannot be met using the standard waveguide size WR28, since the distance between two elements in this case is equal to 11.668 mm. To meet the requirement, waveguide dimension have to be modified in a way, that only dominant mode TE_{10} propagates within the desired frequency range.

The waveguide generated horizontally polarized signal becomes narrower, where the standard WR28 Ka-band waveguide height of $b_{WR28} = 3.556$ mm is reduced to $b_H = 2.9$ mm. While the SWA for vertical polarization is designed as a single ridged waveguide with the reduced width of $a_V = 2.9$ mm. Accordingly, the distance between the two radiating elements is optimized to 6.8 mm. However, during the development process, it became evident that this approach was not viable due to the manufacturing challenges associated with the vertical variant of the designed antenna array. A single ridge-slotted waveguide Ka-band antenna with a center feed necessitates the construction of a complex transition, which must firstly accommodate the available space and secondly ensure optimal input matching. Given that the structure in question remains of an extremely small dimension, it was

not feasible to implement it. This has resulted in a complete alteration to the original specifications for the antenna.

Considering the fabrication possibilities, the fully polarimetric antenna array has been set up from separate antennas, each for one polarization and mounted side by side on the aircraft, as shown in Fig. 2.

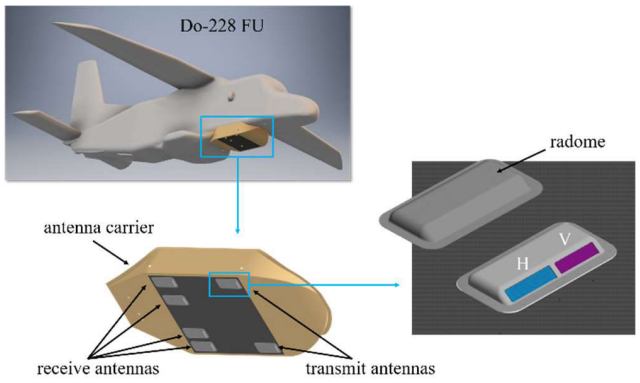

FIGURE 2. Ka-PolInSAR antenna system and its installation framework on the airplane.

B. HORIZONAL POLARIZATION

1) SINGLE ELEMENT

As mentioned in previous section, the single antenna element used for a horizontally polarized signal consists of a modified waveguide with a reduced height, as illustrated in Fig. 3a. The width of the waveguide remains unaltered and is equal to $a_H = a_{WR28} = 7.112$ mm. This dimension consequently yields the guided waveguide wavelength:

$$\lambda_g = \frac{\lambda_0}{\sqrt{1 - (\frac{\lambda_0}{2 * a_H})^2}} = 10.5\ mm \tag{1}$$

The single antenna element is fed centrally by means of a conventional 3 dB H-plane T-junction, as illustrated in Fig. 3b [28], [29]. From a manufacturing perspective, this solution is not straightforward to implement, but is essential for the application described in this work. By employing this approach, the main lobe steering over the frequency is prevented, enabling the creation of a stable radiation pattern with consistent parameters across the desired frequency band. In addition, the bandwidth of such a structure is greater than that of end-feed antennas, further favoring the choice of such feeds. The waveguide is constructed in a standing wave configuration, wherein the short termination is situated at a multiple of an odd quarter of the guided wavelength from the last slot. Consequently, the waves that have been reflected at the terminal point of the waveguide subsequently arrive at the slots in phase. To match the input impedance for the H-plane T-junction the position and size of the pin, located inside the input waveguide, as well as the dimensions of the insets, which are placed on both sides of the input waveguide, can be modified, as shown in detail in Fig. 3c. The pin is positioned precisely at the center of the waveguide in order to ensure an equal distribution of the incoming power to both sides.

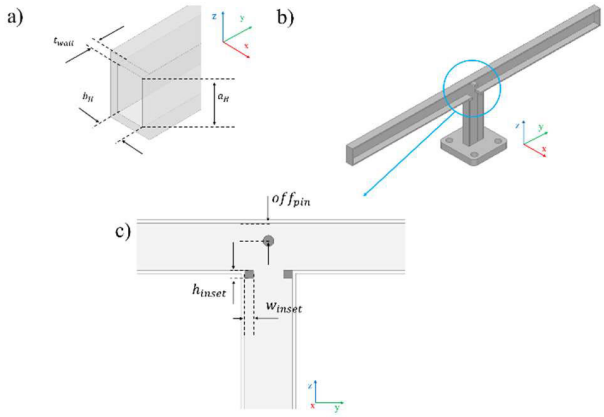

FIGURE 3. The simulated model of an H-plane T-junction used for a horizontally polarized subarray element. a) Waveguide cross-section. Angular view. b) Matching structure.

The antenna element is built with transversal slots cut in the upper narrow waveguide wall, as determined in previous chapter. This configuration results in generation of a horizontal polarized electric field and leads to a low cross-polarization level, since no vertical terms of electric field propagates through these slots. As the wall is of a shorter length than the desired resonant length equal to half free space wavelength $\lambda_0/2$, the slot has been extended to the broad wall of the waveguide in order to satisfy this requirement. The width of the slot has been selected as a compromise between the bandwidth achieved and the impedance behavior at the antenna input. The increasing the slot width results in improved impedance matching but a reduction in bandwidth. An initial value of $\lambda_0/20$ free space wavelength is assumed from the literature and optimized further. The distance between two slots is equal to half the guided wavelength $\lambda_g/2$, which satisfies the requirement for a grating lobe free far-field pattern in this plane. However, the additional structure is necessary to interrupt the current flow, as the transverse slots run parallel to it. There are several methods to excite non-inclined slots. In [30] Ajioka elements are applied, where the use of a pair of transversely placed tilted wires utilized the desired effect. The separation of the wires and their tilt angle control the level of the slot excitation. However, this approach was not implemented, since the wires used for Ka-band antenna would have extreme small diameter. This may lead to radiation pattern disturbance due to the vibration effects on the wires. Another technique to excite the untitled slot is the use of a dielectric plates placed into the slots with conducting strips etched on both sides of it. This approach is outlined in detail in reference in [31]. The issue with this methodology is the difficulty in achieving a stable attachment of the dielectric plates to the waveguide, which presents a significant challenge in the manufacturing process. Furthermore,

the utilization of any dielectric material inevitably results in an increase in losses. In the current design, iris pairs are applied and placed alternately on both sides of each slot to ensure the generation of the equal phase radiated field [32], [33], [34], as shown in Fig. 4. Since the slots are placed with the distance of half-guided wavelength to each other, where the currents run with 180° out of-phase, the iris pairs are placed alternated to each other in order to create an in-phase radiation.

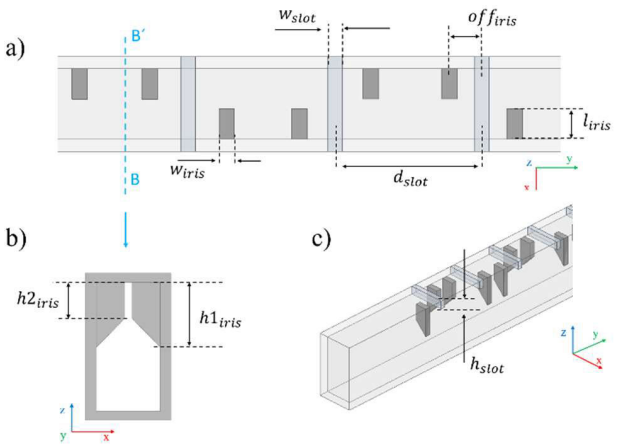

FIGURE 4. The detailed view of a simulation model of a horizontally polarized subarray. a) Slot dimensions. b) Iris pair configuration - side view. c) SWA with iris pairs - angular view.

The impedance matching in this configuration can be achieved through modification of the geometrical dimensions of the iris, as well as adjustment of the slot size to the desired frequency.

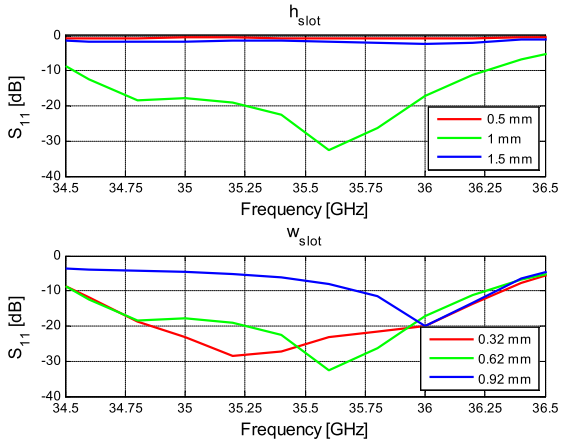

FIGURE 5. The variation of the slot dimension and its influence on the reflection coefficient.

As demonstrated in Fig. 5 and Fig. 6, it is essential to employ both slot and iris pair with precise dimensions in order to ensure optimal impedance matching. Any deviation from this standard will result in inaccurate outcomes and can lead to resonance frequency shifting. The selection of an appropriate slot height is of particular significance in this

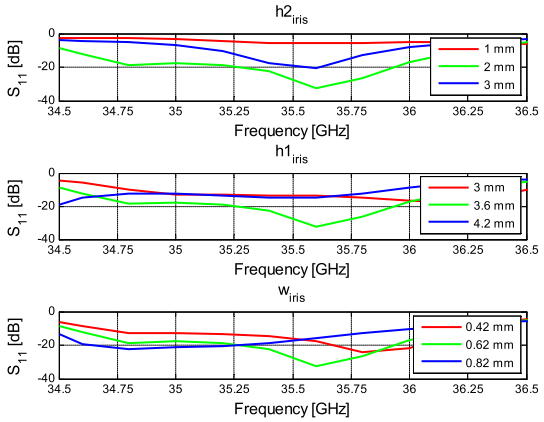

FIGURE 6. The variation of the irises dimension and its influence on the reflection coefficient.

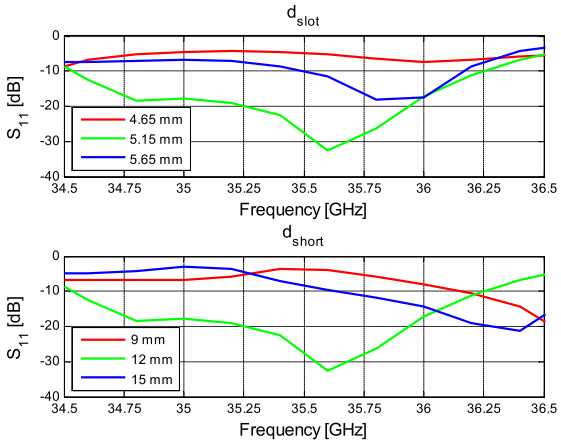

FIGURE 7. The variation of the slot position and its influence on the reflection coefficient.

context. As expected, the resonant frequency change strongly with the variation of this parameter. The influence of the slot position on the reflection coefficient at the antenna input is shown in Fig. 7. The findings of this study demonstrate that discrepancies of desired values result as well in a mismatch.

The requirement on low side lobe level in the azimuth plane demands the implementation of an appropriate current distribution. The slots situated at the center of the waveguide receive more power than those located near the shorted end. To achieve this purpose, the slots are distributed non-uniform about the center of the waveguide, with each pair of mirrored irises exhibiting different geometrical properties. The radiated power through the slot is regulated by changing the position of the iris pair in accordance with the slot and by adjusting the iris length. The movement of the irises serves to regulate the slot's impedance, thereby influencing the subsequent energy emission. The shorter the iris and the closer it is to the slot, the greater slot impedance and thus the energy that can be coupled into the slot. There are a number of current distributions in the literature that are frequently encountered in practice [35]. In order to find a

suitable one for the application presented in this article, the initial current distribution is determined on the basis of the desired parameters, such as SLL and half-power beam width of the antenna, and optimized using a simulation program to obtain required results. Therefore, in order to achieve the desired half-power beam width θ_{Az} and a shaped radiation pattern with low SLL in the azimuth plane, the final single antenna element is composed of 22 slots and a cos-amplitude taper across the subarray element has been implemented and optimized using simulation program and shown in the Fig. 8.

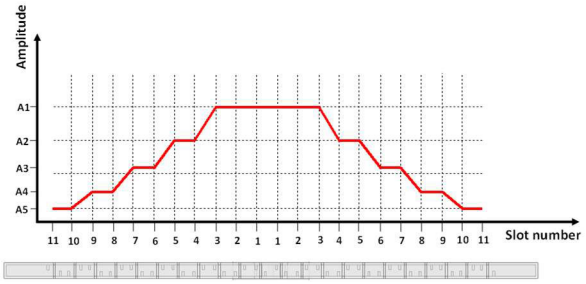

FIGURE 8. The amplitude distribution over the horizontally polarized antenna element.

The power distribution for each slot is listed in Table 2. The parameters have been optimized to produce values that can be implemented from a manufacturing perspective. For this reason, two decimal places have been used.

TABLE 2. The power ratio for horizontally polarized antenna.

Parameter	Value
A1	1
A2	0.9
A3	0.825
A4	0.75
A5	0.675

The model based on the theoretical principles has been generated and optimized in order to achieve the desired parameters. All simulations have been executed using the 3D electromagnetic field simulator Ansys HFSS. In Fig. 9 the simulation model of the horizontally polarized antenna subarray element is shown.

The parameter for the iris configurations to create the desired radiation pattern, are listed in Table 3.

The parameter for the horizontally polarized SWA are summarized in Table 4.

2) ANTENNA ARRAY

The antenna array consists of four antenna subarrays characterized in the previous section and arranged in parallel in H-plane direction. The subarray elements are placed with

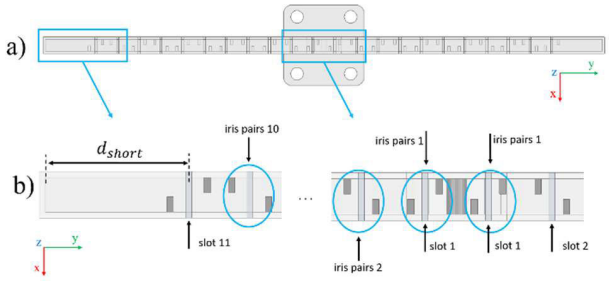

FIGURE 9. The simulation model of a horizontally polarized single antenna element. a) SWA element - top view. b) SWA element - slots configuration.

TABLE 3. The variable parameter for h-polarized single element.

Slot number	Iris length [mm] l_{iris}	Iris offset [mm] off_{iris}
1	1.24	0.9
2	1.24	0.9
3	1.24	0.9
4	1.25	1
5	1.25	1
6	1.26	1.1
7	1.26	1.1
8	1.27	1.2
9	1.27	1.2
10	1.28	1.3
11	1.28	1.3

the distance of $0.8\lambda_0$ with the spacer blocks located 1.8 mm below the radiator level. The spacers serve to simulate the presence of a potential vertically polarized waveguide antenna subarray, which will be implemented in a subsequent phase of the antenna project. The number of elements was selected in order to meet the requirements for both the desired half-power beam width θ_{El} and a shaped radiation pattern in elevation plane. Furthermore, an appropriate amplitude distribution across the four elements is essential for the generation of a diagram with low side lobe level and a wider beam. In order to satisfy these conditions, the power ratio of 0.25:1:1:0.25 across the elements is applied.

The antenna array has been fabricated from aluminum using two supplementary manufacturing techniques, where parts have been manufactured either by eroding or milling process. During the development process, it was determined that this method represents the optimal solution for establishing the antenna. Since the antenna design is very complex,

TABLE 4. The parameter for h-polarized single element.

Variable	Parameter	Value
a_H	waveguide width [mm]	7.112
b_H	waveguide height [mm]	2.9
t_{wall}	wall thickness [mm]	0.5
r_{pin}	pin radius [mm]	0.41
off_{pin}	pin offset [mm]	2.67
w_{inset}	inset width [mm]	1.3
h_{inset}	inset height [mm]	1.25
h_{slot}	slot height [mm]	1
w_{slot}	slot width [mm]	0.5
d_{slot}	slot distance [mm]	5.15
d_{short}	short distance [mm]	12
$h1_{iris}$	iris height 1 [mm]	3.6
$h2_{iris}$	iris height 2 [mm]	2
w_{iris}	iris width [mm]	0.62

it was not possible to manufacture the antenna as a single piece. The fabricated parts were connected by welding.

As an airborne antenna, it is essential that the components retain their electrical properties regardless of environmental influences, by which no corrosion or destruction allowed. In addition to corrosion resistance, the surface must be electrically conductive. To ensure this, a surface treatment with SurTec650 is conducted, which is a well-established chromium passivation process for aluminum in airborne use. The fabricated antenna array is shown in Fig. 10. The upper image presents a possible variation of the installation scenario on a CFK baseplate with the mounting flange, but without a radome for enhanced visual clarity.

3) FEEDING NETWORK

In order to satisfy the requirement for a symmetric amplitude taper over the four elements, a suitable feeding network featuring three sections has been designed and fabricated.

The first section is built as a uniform H-Plane T-junction divider, which splits the incoming power equally to the both output ports. The use of the insets and the septum is applied to match the divider to the input port, as illustrated in Fig. 11a. This process can be controlled by changing both the dimensions of the septum placed symmetrically in the output waveguide and two identical insets placed at the input waveguide. As illustrated in Fig. 12 and Fig. 13, a parametric study of the T-junction has been conducted, demonstrating the impact of varying parameter values on reflection and transmission coefficient. Changing the width of the septum and the height of the insert has a minimal effect on the decoupled power, while the change of the inset width and septum

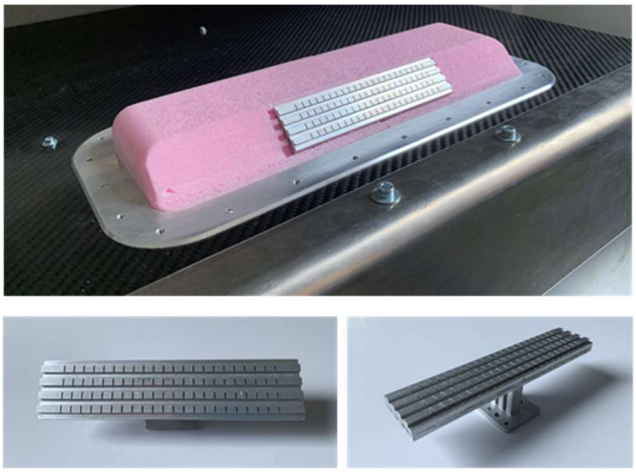

FIGURE 10. The fabricated horizontally polarized antenna array without feeding network.

high influence return loss at the network input significantly. The use of a balanced H-type T-junction results in an equal phase at the output ports. However, a 180° phase difference is observed when the waveguide transitions from a horizontal to a vertical plane. Accordingly, this alteration must be rectified in order to generate a phase-coherent signal at the feeding network output.

The second section is built up as a Bethe-hole directional waveguide coupler [36], [37], which has a single rectangular hole placed in the common broad wall between two waveguides. The coupler configuration is shown in Fig. 11b. The coupling slot must be placed in such a way, that the current flow is interrupted and the electric field can be radiated into the second waveguide. The physical parameters of the coupler, such as the length and width of the coupling hole and its position, determine the coupling intensity. As demonstrated in Fig. 14, the correct size of the coupling slots influences mostly the desired power coupled into the second waveguide. Consequently, it is imperative that the coupling is manufactured with the requisite precision to ensure the desired level of coupling is achieved. The isolated port is short ended, which means that the coupling slot must be placed at a multiple odd quarter guided wavelength $\lambda_g/4$ away from the short end in order to obtain impedance matching. Failure to fulfil this requirement leads to mismatching and, most significantly, to the incorrect power intensity being coupled out of the waveguide, as illustrated in Fig. 15. The four output ports of the network must be placed with the respectively distance to each other, which was already determined in Section A and is equal to 6.8 mm (0.8 λ_0).

The generation of a robust radiation pattern requires a constant phase at the output ports of the network. In order to meet this specification, a third section has been developed in the form of an additional phase balancing element, where the phase compensation is performed for each branch, see in Fig. 11c. The additional phase difference induced partly by changing the waveguide orientation from horizontal to

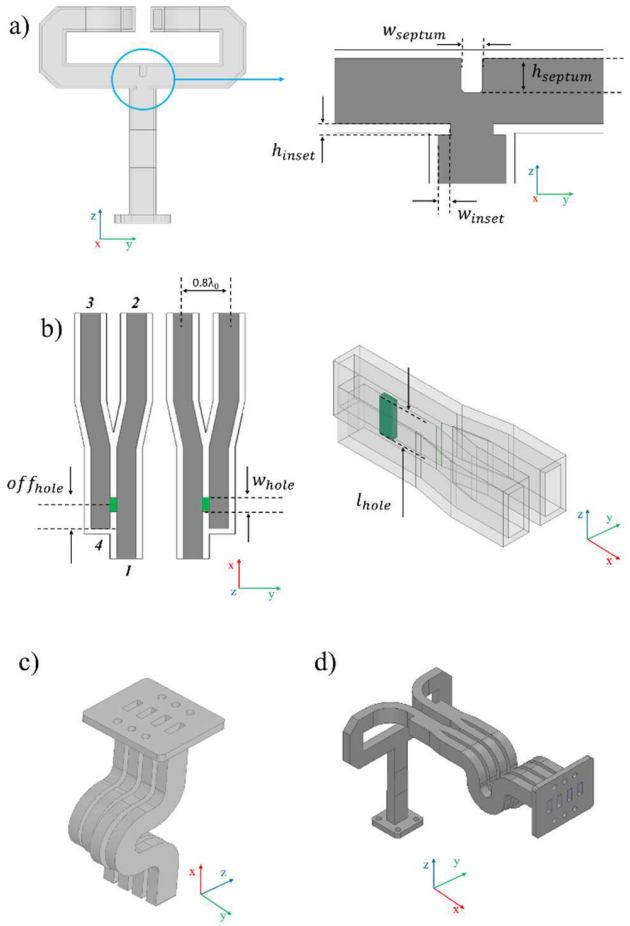

FIGURE 11. The simulated model of a power network for a horizontally polarized antenna array. a) The first section: H-plane T-junction with matching structure. b) The second section: the directional coupler with green marked coupling holes. c) The third section: the phase balancing element. d) Feeding network-simulation model.

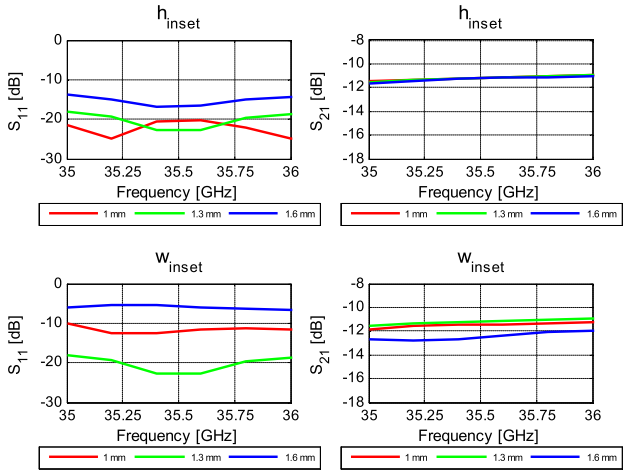

FIGURE 12. The variation of the inset size and its influence on the reflection and transmission coefficient.

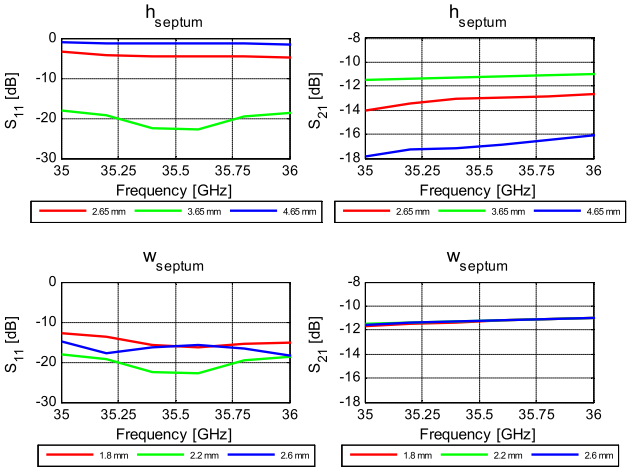

FIGURE 13. The variation of the septum size and its influence on the reflection and transmission coefficient.

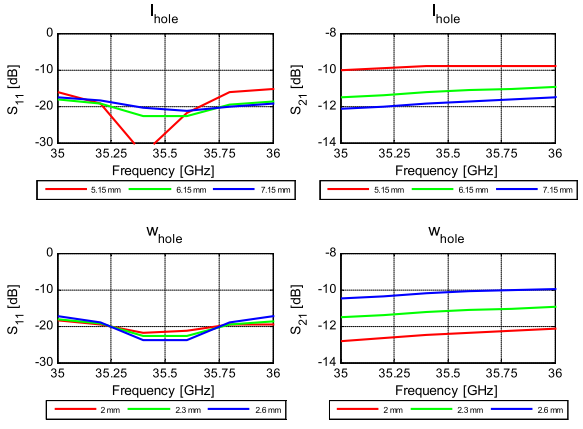

FIGURE 14. The variation of the coupling hole size and its influence on the reflection and transmission coefficient.

vertical, as mentioned before, and partly by directional coupler, has to be adjusted by adding the waveguide sections.

Given that the Ka-band radar system is based on standard Ka-band waveguide dimensions WR28, a tapered transition has been designed to adapt to the standard waveguide width of $\boldsymbol{b_{WR28}} = 3.556$ mm and to make the antenna base compatible to common standards. It supports at the same time the measurements activities for antenna characterization in the Institute Compact Antenna Test Range.

In the Table 5 all relevant parameters for the feeding network used to feed the horizontally polarized antenna are summarized.

The simulation results of the power splitter described in this section are shown in Fig. 16. As illustrated in Fig. 16a, the power network exhibits a well-matched performance across the desired frequency range, with reflection coefficient values below -20 dB within the specified frequency range of 35.25 GHz to 35.75 GHz. Furthermore, the specified power ratio is achieved, with the two outer ports receiving approximately 7 dB less power than the two inner ports, as illustrated in Fig. 16b. The flatness of the output power

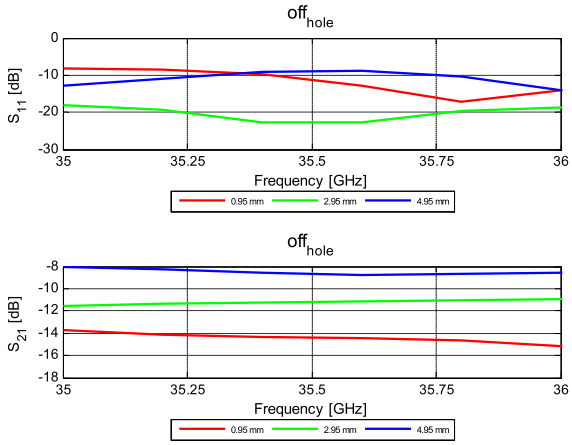

FIGURE 15. The variation of the coupling hole position and its influence on the reflection and transmission coefficient.

TABLE 5. The parameter for h-polarized feeding network.

Variable	Parameter	Value
w_{septum}	septum width [mm]	2.2
h_{septum}	septum height [mm]	3.65
w_{inset}	inset width [mm]	1.3
h_{inset}	inset height [mm]	1.3
w_{hole}	hole width [mm]	2.4
l_{hole}	hole length [mm]	6.15
off_{hole}	hole offset [mm]	4.1

over the desired frequency range is essential for the operation of the antenna. As well as the in-phase nature of the signal, which can be seen in Fig. 16c.

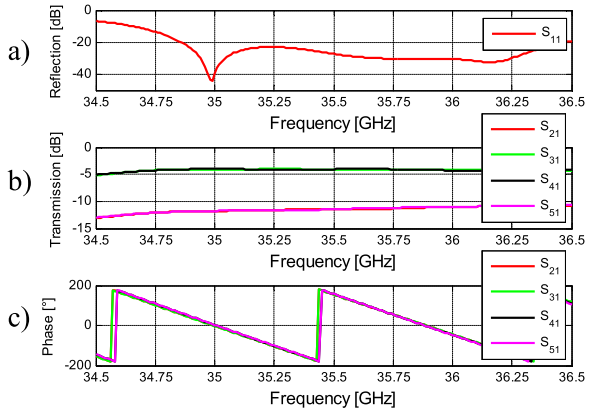

FIGURE 16. The simulated results of the power divider for horizontally polarized antenna array.

The final feeding network has been fabricated using the same manufacturing techniques as for the antenna array. In Fig. 17 the fabricated feeding network with phase balancing element and the transition is presented.

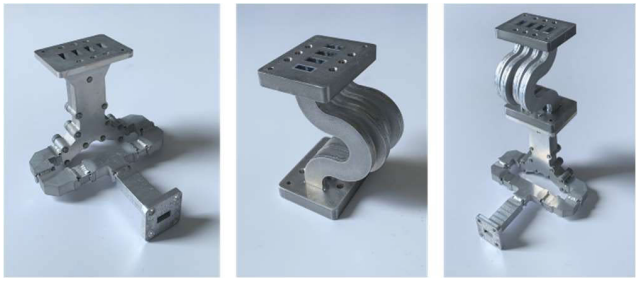

FIGURE 17. The fabricated final feeding network for the horizontally polarized antenna array. a) H-plane T-junction with the directional coupler. b) The phase balancing element. c) Angular view.

C. VERTICAL POLARIZATION

1) SINGLE ELEMENT

As mentioned in section III-A, the vertical polarized slotted waveguide antenna subarray is constructed with longitudinal slots cut in the broad wall, [38], [39], [40], [41]. This slot configuration ensures minimal level of cross-polarization, thereby preventing the generation of horizontal polarized signals. Since the approach to design the antenna based on the standard Ka-band WR28 waveguide leads to grating lobes, the vertically polarized SWA becomes slightly narrower. The SWA width is set to $a_V = 6$ mm with the wall thickness of $t_{wall} = 0.5$ mm, which results in the distance between two waveguides equal to 6.5 mm. The reduction in width has been performed under assumption of propagating only the dominant mode TE_{10} within the desired frequency band. The dimensions of the waveguide have an impact on the vertically polarized guided waveguide wavelength, which can be expressed as follows:

$$\lambda_g = \frac{\lambda_0}{\sqrt{1 - \left(\frac{\lambda_0}{2*a_V}\right)^2}} = 11.9\ mm \quad (2)$$

A central feeding is the optimal configuration, as it ensures a stable radiation pattern across the frequency range, as illustrated in Fig. 18, which is of great importance for SAR applications.

Therefore, an E-plane T-junction has been developed for this objective. The addition of a septum is necessary to ensure optimal matching of the antenna input port. It is positioned symmetrically in the center of the waveguide, thereby facilitating an equal distribution of the input signal across the waveguide. By changing its geometric dimensions, the signal reflection at the input can be regulated. The antenna element is also built in a standing wave configuration, where the last slot is placed at an odd multiple of a quarter guided wavelength $\lambda_g/4$ away from the short, as described in the section B.

The longitudinal slots cut into the broadside wall of a rectangular waveguide are used for creating the vertically polarized antenna element described in this chapter. The slots interrupt the transverse current flow on the wall, forcing the current to travel around the slot. The position of the slot in

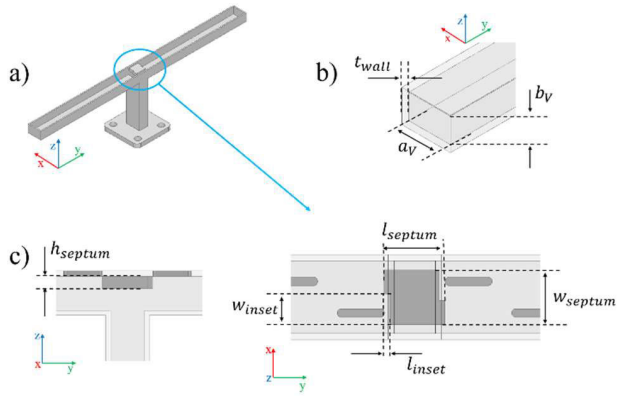

FIGURE 18. The simulated model of an E-plane T-junction used for a vertically polarized subarray element. a) Angular view. b) Waveguide cross-section. c) Matching structure.

relation to the center waveguide line determines the available power and is employed for amplitude tapering. As previously stated in Section B, the slot impedance must be adapted to the characteristic impedance of the waveguide. For here introduced configuration, this can be done by moving the slots from the center line. The closer a slot is positioned from the centerline of the waveguide, the lower its impedance and therefore the lower the radiated energy. In order to achieve a constructive interference of the radiation of the slot, they have to be arranged in phase. In order to avoid formation of unwanted grating lobe in the azimuth plane, the spacing of the slots should fulfil an additional requirement and be less than λ_g. To meet both conditions, the slots are placed with the distance of half guided wavelength and arranged in an alternating sequence relative to the center line of the waveguide. The length of a slot is defined as half the free space wavelength in accordance with the resonant length, which ensures the maximum radiation power from the slot. In order to analyze the influence of slot size and the slot and short distance, a parametric study was carried out, the results of which can be seen in the Fig. 19.

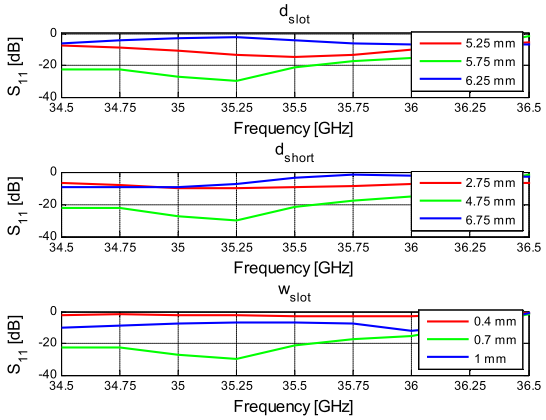

FIGURE 19. The variation of the slot size and position and its influence on the reflection coefficient.

In this instance, the impact of the slot's width is found to be considerably more pronounced in comparison to that of the horizontally polarized antenna, given the slot's location within the E-plane. The distance between the final slot and the short circuit has been established as approximately a quarter of the guided wavelength, a configuration that has yielded favorable outcomes with respect to matching.

The simulation model of the final vertically polarized single antenna element is illustrated in Fig. 20. For proper SAR operations both antenna pattern, in horizontal and vertical polarization must be of an identical shape.

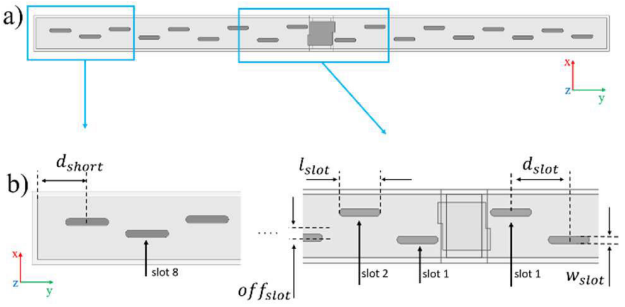

FIGURE 20. The simulated model of a vertically polarized single antenna element. a) SWA element - top view. b) SWA element - slots configuration.

A suitable amplitude distribution must be applied in order to achieve the desired half-power beam width in the azimuth plane θ_{Az} and simultaneously to obtain a low side lobe level. The antenna can be matched to the characteristic impedance of the waveguide by offsetting the slots from the centerline. The position of the slot determines its impedance and therefore the amount of energy radiated through it. The further a slot is from the centerline of the waveguide, the lower its impedance and the less energy it will radiate. In order to feed the antenna unevenly, the slots in the center of the waveguide must receive more power than those at the end. To ensure that the total impedance of the slots is adapted to the impedance of the waveguide, the slot lengths must also be adapted. The table in [35] is used to select an appropriate current distribution to produce the desired opening angle and low side lobe level. In order to meet the requirements from the Table 1, the vertically polarized antenna subarray consists of 18 slots and has been provided with a cos-amplitude taper shown in Fig. 21.

The power distribution values for each slot within the single antenna element for vertically polarized element are listed in Table 6.

Since the waveguide used to generate the vertical polarization has a different cross section to the antenna element that generates a horizontally polarized signal, a smaller number of slots in the azimuth plane is required to achieve the desired radiation pattern with the same electrical parameters as for horizontal polarization.

The parameter values for the vertically polarized subarray are summarized in the Table 7 below.

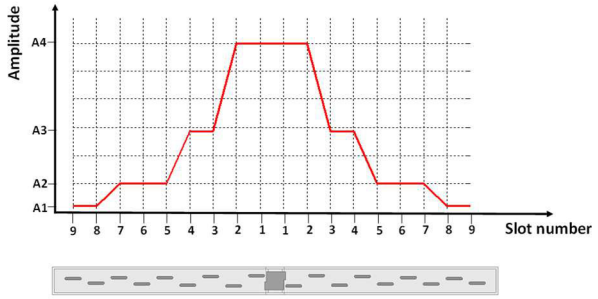

FIGURE 21. The amplitude distribution over the vertically polarized antenna element.

TABLE 6. The power ratio for vertically polarized antenna.

Parameter	Value
A1	1
A2	0.675
A3	0.5
A4	0.425

TABLE 7. The parameter for v-polarized single element.

Variable	Parameter	Value
a_V	waveguide width [mm]	6
b_V	waveguide height [mm]	3.556
t_{wall}	wall thickness [mm]	0.5
h_{septum}	septum height [mm]	1.3
w_{septum}	septum width [mm]	4.5
l_{septum}	septum length [mm]	5.25
l_{inset}	inset length [mm]	0.5
w_{inset}	inset width [mm]	2.25
w_{slot}	slot width [mm]	0.7
d_{slot}	slot distance [mm]	5.75
d_{short}	short distance [mm]	4.75

The parameters for the slot dimension and position are listed in Table 8.

2) ANTENNA ARRAY

The proximity of the elements in the E-plane direction gives rise to the formation of strong surface currents, which in turn give cause to the generation of strong mutual coupling effects. Such impacts have the effect of disturbing the desired pattern and reducing the performance of the antenna. There are a number of potential methods for interrupting these currents. In [42] electromagnetic band-gap structure (EBG) proposed as a possible solution. The periodic EBG structures exhibit band-gap feature in the suppression of surface wave propagation. However, such an application requires an appropriate spacing between the array elements. An alternative approach to reducing mutual coupling between the elements is presented in [43], where the use of inside grooves interrupts the current flow. Since the dimension of such a structure for a Ka-band system would be extremely small, the conductive walls were insert on both sides of every single antenna subarray, as shown in Fig. 22 below. At the same time this wall simulates the presence of a horizontally polarized subarray as well for a future configuration.

TABLE 8. The variable parameter for v-polarized single element.

Slot number	Slot length [mm] l_{slot}	Slot offset [mm] off_{slot}
1	3.37	1.3
2	3.37	1.3
3	3.385	1.1
4	3.385	1.1
5	3.4	0.8
6	3.4	0.8
7	3.4	0.8
8	3.45	0.55
9	3.45	0.55

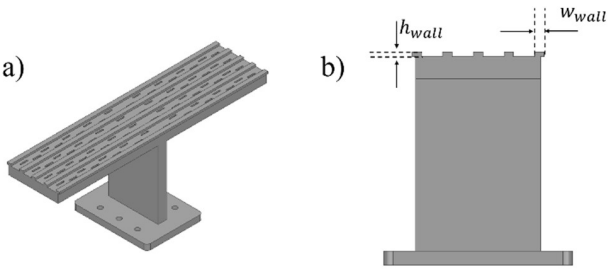

FIGURE 22. The simulated model of a vertically polarized antenna array. a) angular view. b) side view - conductive walls with their dimensions.

The parameter values for the design with the conductive walls are listed in the Table 9 below.

TABLE 9. The conductive wall parameter.

Variable	Parameter	Value
w_{wall}	conductive wall width [mm]	2
h_{wall}	conductive wall height [mm]	1

The simulated results for both designs, with and without the conductive walls, are compared by the means of return loss levels in Fig. 23. In the absence of conducting walls, the input impedance is moderate across the entire frequency range. The addition of this structure results in a significant improvement in matching, as illustrated by the red curve.

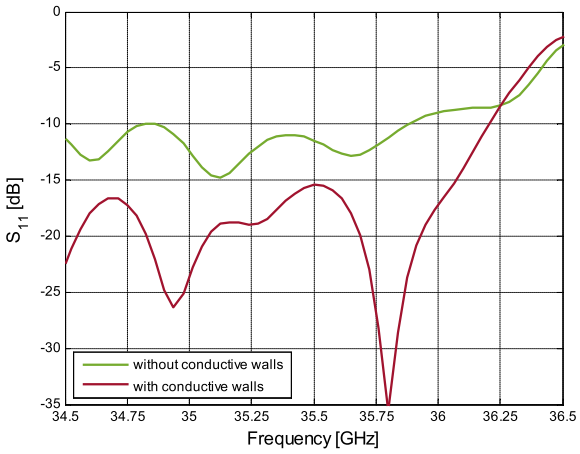

FIGURE 23. The simulated results of reflection coefficient for vertically polarized antenna array and the influence of conductive walls.

The effect of the mutual coupling is even more clearly visible in the principal cuts of the antenna main beam pattern. The simulation results for both configurations are shown in Fig. 24.

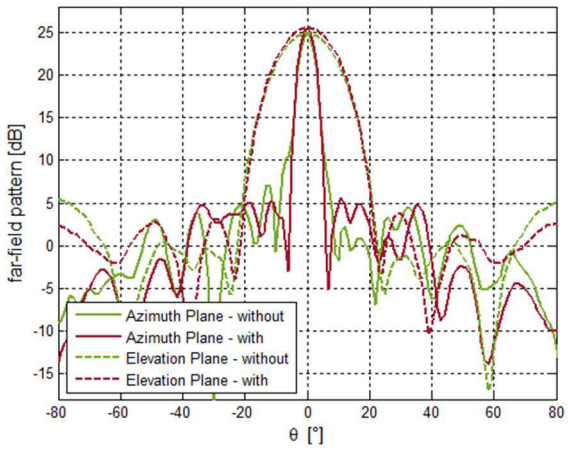

FIGURE 24. The simulated co-polarization far-field pattern for azimuth- and elevation- plane for the center frequency f_0 =35.5GHz and the influence of the conductive walls.

In addition to a reduction in antenna gain of approximately 0.63 dB, the patterns exhibit a loss of symmetry and an increase in side lobes. As a consequence of the vertical polarization, the E-plane cut in the azimuth direction is particularly susceptible to influence.

In order to more accurately represent the impact of the conductive walls, the surface current distribution pattern at the center frequency in two-dimensional representation was plotted and illustrated in Fig. 25.

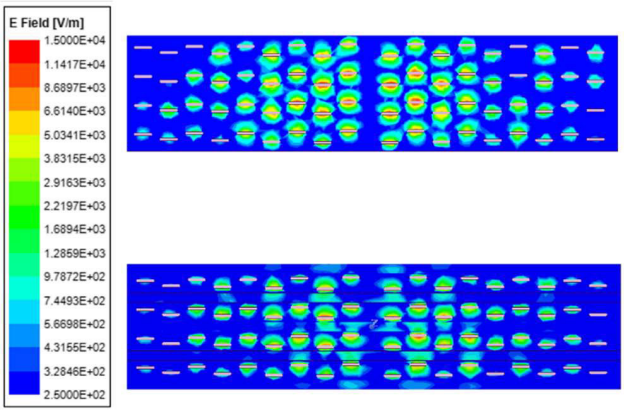

FIGURE 25. The simulated surface current distribution plotted at center frequency f_0 =35.5GHz. without the conductive walls (upper diagram) and with the conductive walls (bottom diagram).

The elements in elevation plane must be fed non-uniformly in order to achieve a desired radiation pattern in the elevation plane with a low side lob level and a suitable half-power beam width θ_{El}. In order to satisfy both of the aforementioned requirements, it is necessary to apply a power ratio of 0.33:1:1:0.33 across the four individual antenna subarray elements. The antenna array has been manufactured applying the same technological methods as the antenna for horizontal polarization, which are the eroding and milling fabrication and shown in Fig. 26.

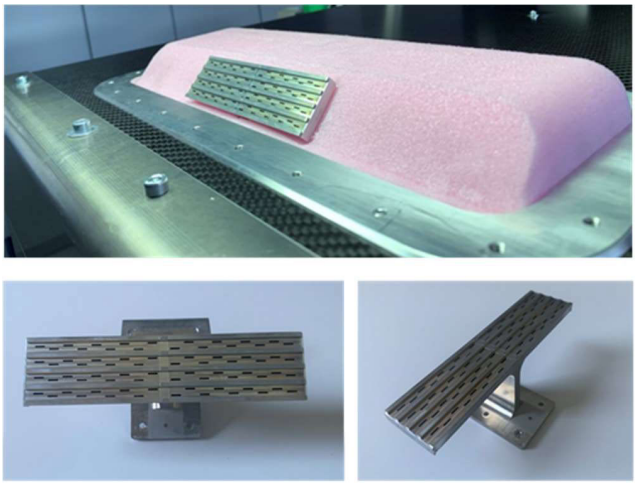

FIGURE 26. The fabricated vertically polarized antenna array.

3) FEEDING NETWORK

To obtain the desired amplitude distribution, the feeding network for this polarization consist of three H-plane T-junctions and can be divided into two sections. The simulated model of the power splitter used for vertically polarized antenna array is illustrated in Fig. 27.

The first part consists of a uniform H-plane T-junction, which divides the input power equally into the transverse

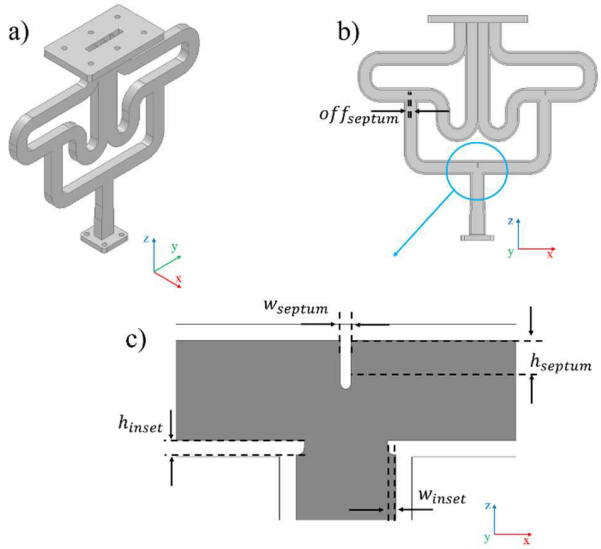

FIGURE 27. The simulated model of a feeding network for vertically polarized antenna array. a) Angular view. b) Front view with marked matching structure. c) The matching structure in detail.

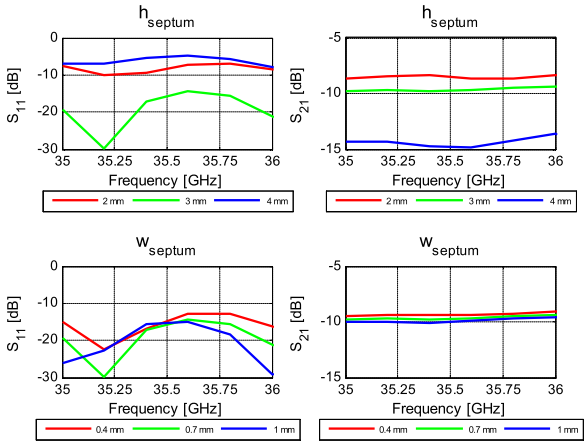

FIGURE 28. The variation of the septum size and its influence on the reflection and transmission coefficient.

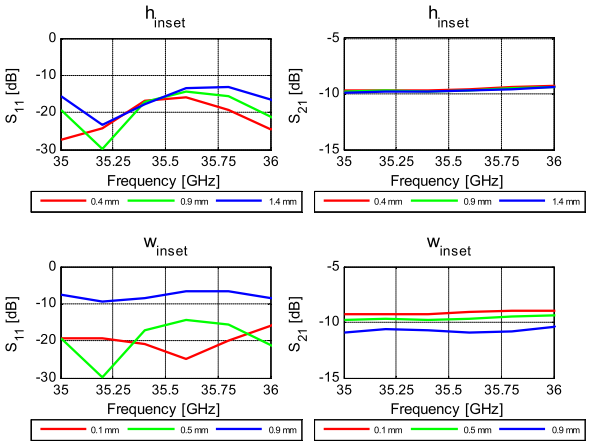

FIGURE 29. The variation of the inset size and its influence on the reflection and transmission coefficient.

waveguide section with equal phase at the output ports. In order to serve this purpose, the septum placed inside the waveguide must be located centrally.

The second section of the feeding network is constructed of two H-plane T-junctions of equal construction, which distribute the power in an unequal manner. This results in the edge element receiving less power than the middle element. By shifting the septum sideways, the power distribution to the waveguide output can be regulated. The input impedance matching for each H-plane T-junction employed for this approach is achieved through the adaption of the geometric dimensions of the septum, as well as by adjusting the width and height of the insets located on either side of the input waveguides. A parametric study was conducted in order to ascertain the impact on network functionality. Fig. 28 and Fig. 29 show the variation of septum and inset size respectively. The results obtained demonstrate a tendency towards similarity with a horizontally polarized network. It was established that the height of the septum and the width of the inset, specifically, have a significant impact on the resonance behavior of the network. However, alterations in the width of the septum and the height of the inset appear to exert a negligible influence on the resonant frequency and the power distribution. In order to attain signals with a consistent phase, the waveguides must be calibrated to the corresponding electrical lengths.

The relevant parameter values for the feeding network utilized to feed the vertically polarized antenna array are presented in Table 10.

Since the waveguide size does not correspond to WR28 standard waveguide dimension, it is necessary to design and adapt a suitable transmission at the input waveguide in order

TABLE 10. The parameter for v-polarized feeding network.

Variable	Parameter	Value
w_{septum}	septum T-Junction width [mm]	0.7
h_{septum}	septum T-Junction height [mm]	3
off_{septum}	septum offset [mm]	0.8
w_{inset}	inset width [mm]	0.5
h_{inset}	inset height [mm]	0.9

to enable the measurement and adjustment of the antenna to the system.

In Fig. 30 simulation results of the power splitter are plotted.

The impedance at the power divider input is well matched over the desired frequency range and remains at the -20 dB level, which can be observe in Fig. 30a. The power distribution stays constant over the frequency and fulfill the specification, as shown in Fig. 30b. The power difference

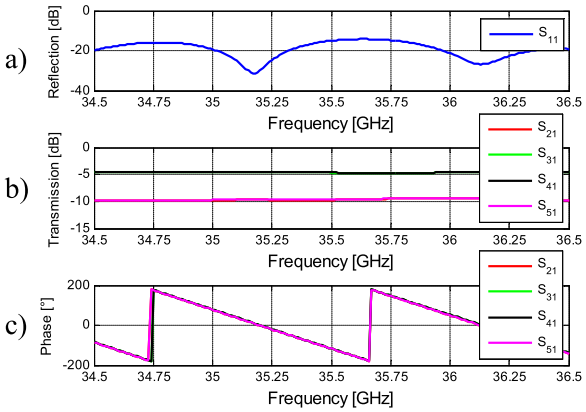

FIGURE 30. The simulated results of the power divider for vertically polarized antenna array.

between the inner and the output ports is approximately 5 dB, which is in accordance with the desired specifications. Furthermore, the requirement for an in-phase signal at the power divider output ports is fulfil, as evidenced in Fig. 30c, where the achieved phase over the frequency range is plotted.

The final feeding network developed for vertically polarized antenna array has been manufactured by the same supplier using both eroding and milling fabrication methods. The manufactured network is illustrated in Fig. 31.

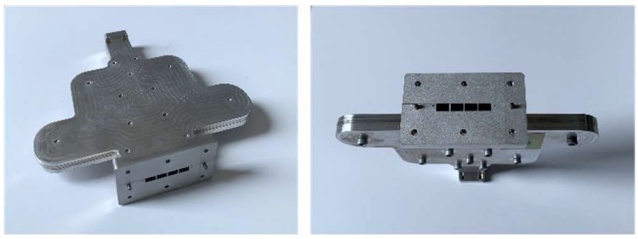

FIGURE 31. The fabricated final feeding network for the vertically polarized antenna array.

IV. MEASUREMENT RESULTS

Based on the simulation models represented above, both antennas, inclusive of the feeding networks, have been fabricated. In order to ascertain whether the requisite antenna specifications have been met, the measurements obtained from the manufactured antenna arrays for both horizontal and vertical polarization are presented in the following section.

During the measurement, the antennas are mounted on a carbon-fibre-reinforced polymer (CFRP) base plate. It simulates the environment in which SAR operations are conducted. The primary objective of the antenna configuration is to perform measurements in interferometric modes, wherein the phase difference in the received signals is analyzed to generate the SAR product. Due to the high frequency and small wavelength, the physical position of the receive antennas in relation to one another is of critical importance for the application. The airborne use case results in temperature changes between 60° and 70°. The CFRP base plate is designed to compensate for linear expansion over temperature.

In order to facilitate the SAR application, it is necessary to implement a side-looking geometry. The antennas are mounted at an angle specific to the base plate and affixed to an aluminum flange. During operation, the flange will be covered with an ABS radome. The available internal space is filled with Austrotherm XPS, which has an extremely low dielectric constant and will not affect the electromagnetic performance of the antenna installation.

FIGURE 32. The final antenna array arrangement on the CFRP plate.

The edge of the CFRP base plate, situated at the front of the antenna, is furnished with a bended sheet of aluminum, which serves to simulate the aerodynamic cover of the antenna carrier. Consequently, the final configuration of the installation scenario during operations is emulated in antenna measurements at the Institute Compact Antenna Test Range, as illustrated in Fig. 32.

As the Ka-PolInSAR system will be used in various airborne measurement campaigns in the future, it is essential that the design ensures unaltered behavior under all environmental conditions. Therefore, the antennas are safeguarded against meteorological conditions, including precipitation, snow, ice, dust, and other particulates that may be encountered during take-off, landing, or throughout the duration of the flight. A radome is implemented to cover the antennas and provide an aerodynamic enclosure as well. The material for the radome must be selected in a way that disturbing the electromagnetic wave is minimized. This is achieved by choosing a material with low dielectric permittivity and a precisely calibrated thickness. For here described application a S-Polytec ABS/ASA has been used, which is resistant to weathering. The ASA/ABS sheets owe this to a special ASA top layer that is resistant to UV radiation. It is of paramount importance to ascertain the optimal thickness and distance to the antenna radiating surfaces. The optimal result was obtained by utilizing a standardized S-Polytec ABS/ASA material with a thickness of 2 mm and a distance to the antennas of 4 mm and 3 mm, respectively, for horizontally and vertically polarized antennas. The radome is formed into the desired shape using a thermoforming mold, with consideration given to the change in thickness of the material during

the molding process. The construction employed to create a suitable radome is illustrated in Fig. 33.

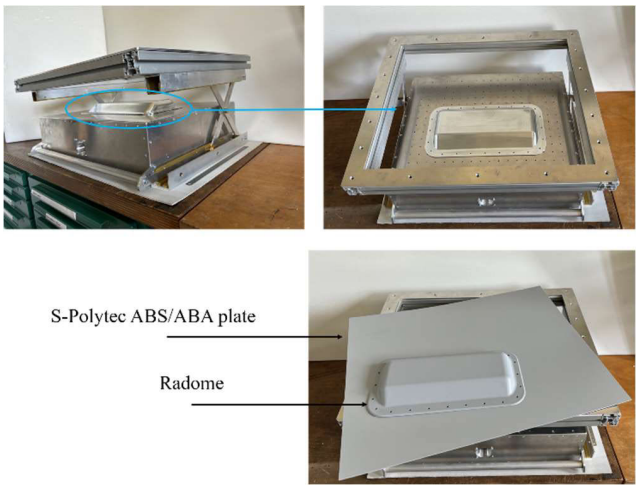

FIGURE 33. The thermoforming construction with the S-Polytec ABS/ABA plate and the finished radome.

In order to ascertain the quality of the antenna, first the reflection coefficient at the antenna input was measured using a Keysight Field Fox Microwave Analyzer, see Fig. 34a. The S11 value is in good agreement with the expected result, although the values for horizontal polarization show slightly more reflections at the input of this antenna within the desired frequency range. Nevertheless, the outcomes remain within an acceptable range. The reflection coefficient values for both antennas are at a level better than −13 dB and −15 dB for horizontal and vertical polarization respectively. The measured bandwidth is 5.6 % and 6.4 % relative to the center frequency. The isolation between the H- and V- polarization is greater than 55 dB, see the Fig. 34b.

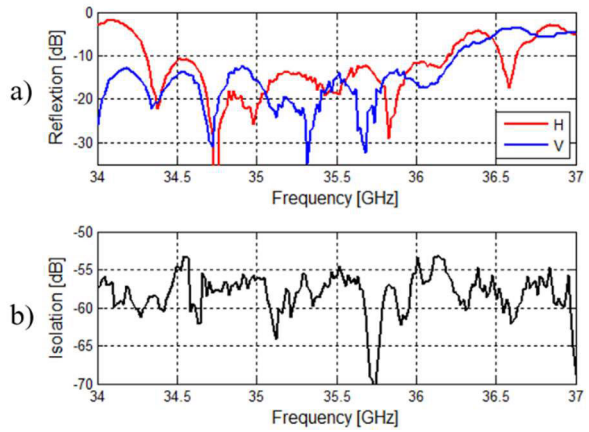

FIGURE 34. The measured reflection- and isolation coefficient of the final antenna arrays (H - horizontally polarized array, V - vertically polarized array).

Following the completion of the laboratory test, the radiation characteristics are then measured in the DLR Compact Antenna Test Range (CATR) [44], as shown in Fig. 35.

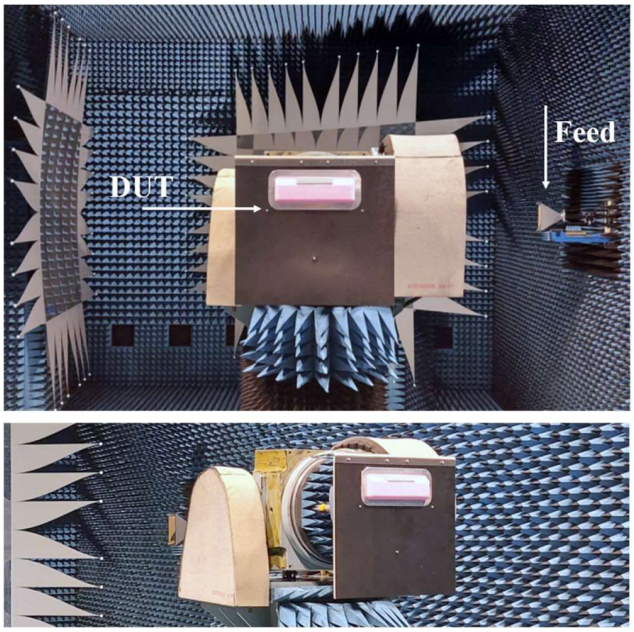

FIGURE 35. The measurement arrangement at CATR. For better visibility, the radome is removed in this image.

As determined in section II, the required beam width in the flight direction (azimuth plane) should have a narrow shape with a maximum half-power beam width of $\theta_{Az} \leq 5°$. As illustrated in Fig. 36, both antennas satisfy this criterion admirably, exhibiting measured parameter values of 4.6° and 4.9° at the center frequency. Furthermore, the required SLL of 18 dB has been fulfilled as well. However, the vertically polarized antenna shows better suppression and achieves values around 22 dB below the main lobe. The cross-polarization levels for both antennas are less than 38 dB, which fulfils the specified requirement for this parameter.

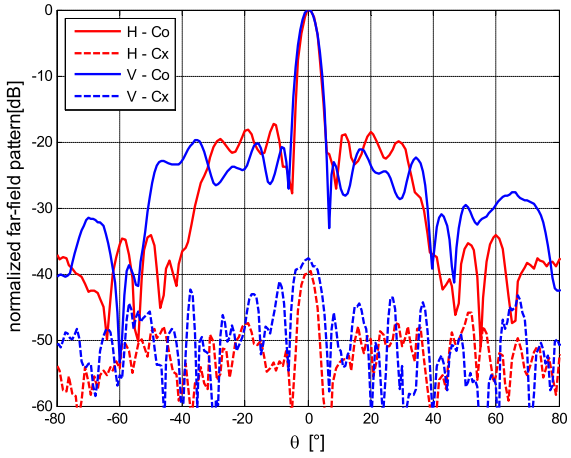

FIGURE 36. The measured normalized co- and cross- polarization far-field pattern of the final antenna arrays at the center frequency f_0 =35.5GHz in azimuth plane.

In Fig. 37 the normalized co- and cross-polarization far-field patterns measured at the center frequency in the

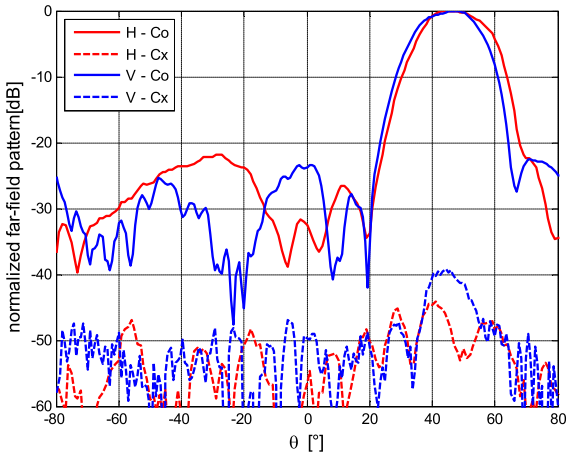

FIGURE 37. The normalized measured co- and cross- polarization far-field pattern of the final antenna array at center frequency f_0 =35.5GHz with the mechanical steering at 45° in elevation plane.

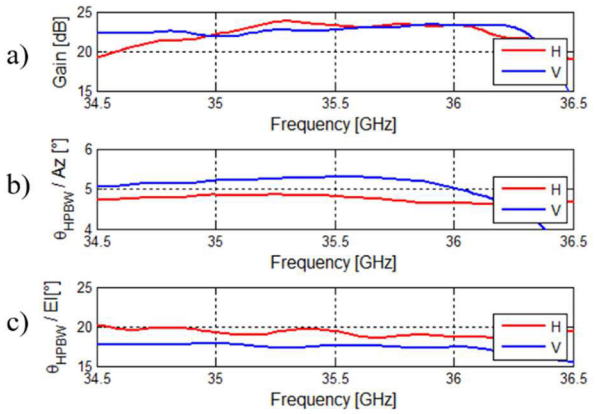

FIGURE 38. The measured total gain over the frequency, the measured half-power beam width in azimuth plane θ_{Az} over the frequency and the measured half-power beam width in elevation plane θ_{El} over the frequency.

elevation plane including the mechanical beam steering have been plotted. The demand on SLL lower than 18 dB is well reached for both antennas. The cross-polarization level is situated at approximately 40 dB below the main lobe for both antennas. The slight variation in this parameter can be attributed to the alignment of the azimuth cut at the elevation main beam direction. A slight discrepancy in pointing can give the impression of a difference in cross-polarization levels. For the desired application for the antennas used for SAR operations, additional requirements to the shape of the elevation pattern must be fulfilled. When mounted underneath the fuselage of an aircraft, the nadir direction delivers a strong echo performance and should be suppressed by the antenna pattern. Additionally, the opposite side to the illuminated range on the ground beneath the flight path should be considered. The area of interest falls within the angular range of 25° to 60° off-nadir. It is necessary to suppress all other directions, as illustrated in Fig. 37.

In order to provide a comprehensive overview of the antennas' performance across the entire frequency band, the variation in antenna gain and half-power beam width for both azimuth and elevation planes are presented in Fig. 38.

The antenna array gain varies between 22 dBi and 23.5 dBi within the desired frequency band. The necessity for a maximum gain is justified by the significance of attaining a favorable signal-to-noise ratio (SNR). In particular, within this frequency range, the use of a maximum-gain antenna is of paramount importance, as the free-space attenuation reduces the signal strength, thereby leading to a poor signal-to-noise ratio (SNR), which in turn results in the generation of low-quality synthetic aperture radar (SAR) images. The half-power beam width in the azimuth plane, which is depicted in Fig. 38b, demonstrates remarkable stability for both antennas. The beam width changes only 0.2°. In the elevation plane the change of 1° for horizontally and 0.5° for vertically polarized antenna is still in the specified range, see Fig. 38c.

The far-field patterns for co- and cross-polarization for both antennas measured for the azimuth and elevation planes at low (35.25 GHz), center (35.5 GHz) and high (35.75 GHz) frequencies have been plotted and illustrated in Fig. 39, Fig. 40, Fig. 41 and Fig. 42, respectively. The results of the measurements at various frequencies correspond with the specifications. It can be observed that there is a slight increase in the sidelobe level at higher frequencies in the azimuth plane for vertical polarisation, which is caused by frequency-dependent slots and manufacturing tolerances. The manufacture of the antenna components with the required accuracy represents a significant challenge and a crucial aspect of the overall performance. A number of fabrication methods were evaluated in order to identify a suitable and reliable approach.

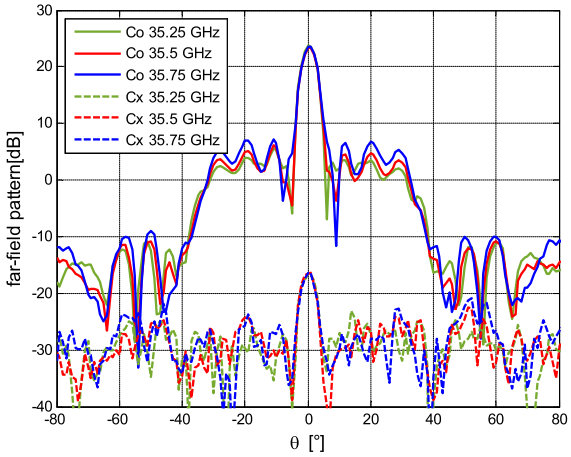

FIGURE 39. The measured co- and cross-polarization far-field pattern of the horizontally polarized final antenna array in elevation plane for low, center and high frequency band values.

In Table 11 a number of measured parameters for both antennas calculated at center frequency are summarized.

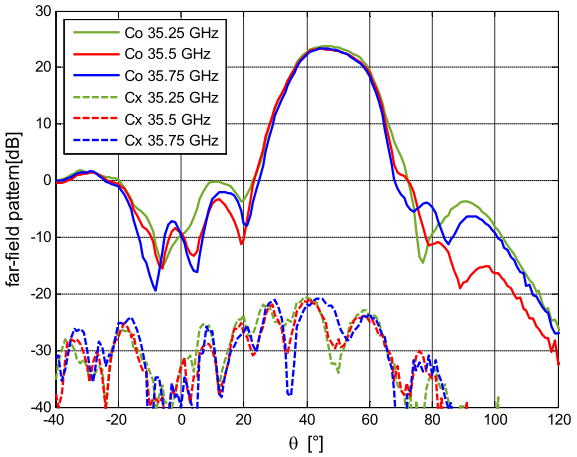

FIGURE 40. The measured co- and cross-polarization far-field pattern of the horizontally polarized final antenna array in elevation plane for low, center and high frequency band values.

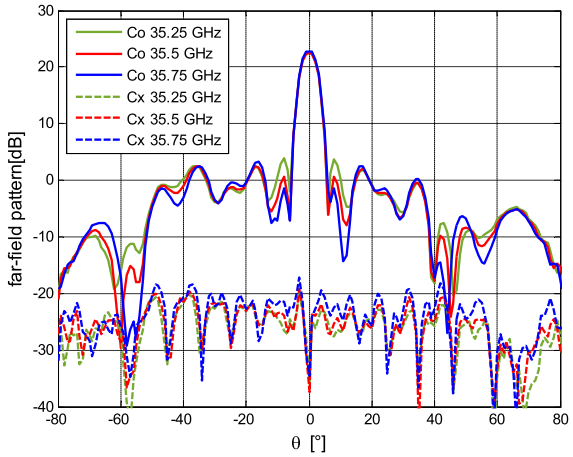

FIGURE 41. The measured co- and cross-polarization far-field pattern of the vertically polarized final antenna array in Azimuth plane for low, center and high frequency band values.

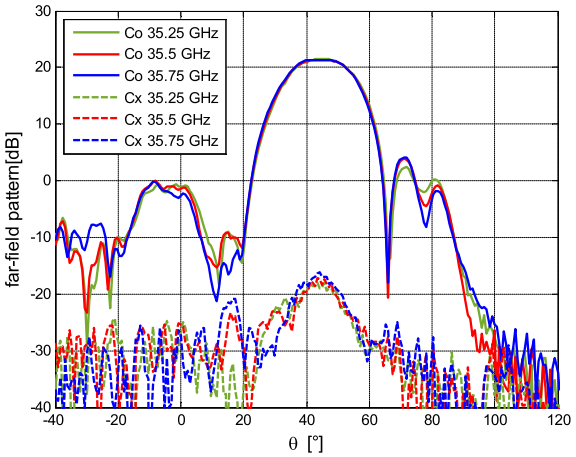

FIGURE 42. The measured co and cross-polarization far-field pattern of the vertically polarized final antenna array in azimuth plane for low, center and high frequency band values.

TABLE 11. The antenna array measured parameter.

Variable	Parameter	H	V
B	bandwidth [GHz]	2	2.25
G	gain [dBi]	23.3	22.7
θ_{Az}	half-power beam width in azimuth [°]	4.6	4.9
θ_{El}	half-power beam width in elevation [°]	21.6	20.6
SLL	side lobe level in azimuth [dB]	18	20
SLL	side lobe level in elevation [dB]	25	20
-	cross-polarization level in azimuth [dB]	40	38
-	cross-polarization level in elevation [dB]	40	40
-	opposite swath suppression [dB]	25	25

V. COMPARISON WITH OTHER WORKS

The primary challenge in the development of antennas operating at higher frequency bands, which are used for airborne SAR applications, is to design an antenna that fulfils all requirements and is simultaneously feasible from a manufacturing perspective. In order to provide an overview of the performance achieved with the proposed work, a comparison with other Ka-band antennas is presented in Table 12.

It is noteworthy, that the antenna presented in this work is one of the few that operate in a dual-polarization mode and at the same time is fed by an non-uniform feeding networks in both planes in order to achieve a desired radiation pattern with low side lobe- and cross-polarization level. To the best author knowledge, only antennas presented in [25], [45], and [47] provide similar properties. Neverthless, both antennas introduced in [45] and [47] are end-fed SWAs, which can be an issue regarding the frequency stability, since this configuration lead to mainlobe streering within the relevant bandwidth.

The antenna described in [25] and constructed utilising SIW technology provides a very high cross-polarization level, which is not accepted for the application characterised in this article. A further requirement for antennas used in an airborne SAR system is that they should have good aerodynamic properties. This can be achieved technically mainly by using low-profile antennas, since the available space is often limited. Thus, the use of horn antennas presented in [8] and [51] is not always possible. In [45] and [48] the gap waveguides are used to create a Ka-band antenna array. Despite the antenna described in [45] being dual-polarised, the implementation of a non-uniform amplitude distribution appears to be highly challenging and has yet to be tested.

TABLE 12. Comparison of the proposed work with other ka-band antennas.

Reference	Polarization	Array elements	Gain [dB]	Bandwidth [GHz]	Amplitude tapering	Feeding type	Cross-Polarization Level [dB]	Frequency of operation [GHz]	Antenna type
[45]	dual linear	7x12 (V) 8x12 (H)	20 (V) 25 (H)	1	non-uniform	end-fed	40	35	SWA
[46]	dual linear	8x8	27	1.5	uniform	center-fed	50	30.25	GAP Waveguide
[47]	dual linear	8x10 (V) 9x10 (H)	24.8 (V) 25.4 (H)	0.658 (V) 0.688 (H)	non-uniform	end-fed	25	35	SWA dual-band
[48]	single	2x8	19.98	3	uniform	center-fed	25	35	SWA
[49]	single	4x9	24	1.5	uniform	end-fed	30	28	Groove-GAP waveguide
[50]	single	1x13	12.3	3.5	non-uniform	end-fed	NA	35.5	SWA
[51]	single	32 x 2x9	34	1.25	uniform	center-fed	NA	35.75	SWA
[52]	single	NA	NA	0.4	NA	NA	NA	35	Horn antennas
[8]	single	1x2	20	8	non-uniform	NA	NA	34	Horn antennas
[2]	dual linear	NA	22	0.5	non-uniform	NA	25	35.75	SWA
[20]	single	8x8	15.6	1.4	uniform	quad channel RFIC	NA	30	Slotted SIW
[21]	single	1x16	15.64	1	non-uniform	center-fed	15	35	Slotted SIW
[22]	single	8x20	28.7	1	non-uniform	end-fed	NA	34.8	Slotted SIW
[23]	single	8x14	19.1	2.3	non-uniform	end-fed	NA	34	Slotted SIW
[24]	dual linear	unit cell	6.2 7.4	0.55 0.75	uniform	-	NA	20 30	SIW Patch Antenna
[25]	dual linear	4x4	NA	0.48	non-uniform	center-fed	15	35	Slotted SIW
[26]	dual linear	8x16	24	1	uniform	center-fed	13	35	Slotted SIW
This work	**dual linear**	**4x18 (V) 4x22 (H)**	**22.7 (V) 23.3 (H)**	**2.25 (V) 2 (H)**	**non-uniform**	**center-fed**	**40**	**35.5**	**SWA**

VI. CONCLUSION

This article presents the development of a fully polarimetric antenna array for the DLR future Ka-PolInSAR system. The array antennas for both linear vertical and horizontal polarization were designed using slotted waveguide antenna technology and placed side by side on the aircraft fuselage. The antenna models were created based on the theoretical fundamentals and subsequently optimized in order to fulfil the requisite specifications.

The prototypes were manufactured using eroding and milling fabrication techniques and measured in order to verify compliance with the specifications. As the antenna arrays for both polarizations were developed separately, the challenge was to design the antennas in a manner that would ensure their parameters were similar. This was deemed an important request, as it would facilitate the generation of a high-quality SAR image product.

The vertically polarized antenna array consists of four subarrays and was designed with longitudinal slots cut in the broad waveguide wall and fed by a feeding network based on two stage H-plane T-junction.

The results of the measurements taken on both antennas are presented in this work, and a satisfactory level of agreement with the specifications was achieved. The results demonstrate the efficacy of the antenna array in achieving a maximum gain with minimal cross-polarization and side lobe level, as well as an adequate nadir and opposite swath suppression.

The challenge of developing two different antennas that ultimately produce the same radiation pattern was successfully overcome, with only minor discrepancies between the achieved parameters.

It has been demonstrated that the manufacturing aspect of development tasks assumes greater significance with increasing frequency. 3D metal printing appears to offer a potential

solution to the challenges encountered in the manufacturing process. However, it has been observed that there are higher losses due to surface imperfections at Ka-band. It can be concluded that the more traditional manufacturing processes are still preferred for optimal performance in antenna applications.

REFERENCES

[1] A. Moreira, P. Prats-Iraola, M. Younis, G. Krieger, I. Hajnsek, and K. P. Papathanassiou, "A tutorial on synthetic aperture radar," *IEEE Geosci. Remote Sens. Mag.*, vol. 1, no. 1, pp. 6–43, Mar. 2013.

[2] F. Speziali, C. Trampuz, S. Placidi, L. C. I. Hendriks, M. Ludwig, and A. Meta, "Development of the multichannel interferometric Ka-band airborne SAR instrument (KaSAR)," in *Proc. 12th Eur. Conf. Synth. Aperture Radar (EUSAR)*, Jun. 2018, pp. 1–5.

[3] P. A. Rosen, S. Hensley, K. Wheeler, G. Sadowy, T. Miller, S. Shaffer, R. Muellerschoen, C. Jones, H. Zebker, and S. Madsen, "UAVSAR: A new NASA airborne SAR system for science and technology research," in *Proc. IEEE Conf. Radar*, Verona, NY, USA, Jun. 2006, pp. 1–12.

[4] O. R. du Plessis and P. Dreuillet, "The ONERA airborne multi-frequency SAR imaging systems," in *Proc. Int. Conf. Radar*, Adelaide, SA, Australia, Sep. 2013, pp. 85–90.

[5] R. Baque, P. Dreuillet, and H. Oriot, "Sethi: Review of 10 years of development and experimentation of the remote sensing platform," in *Proc. Int. Radar Conf. (RADAR)*, Toulon, France, Sep. 2019, pp. 1–5.

[6] S. R. Rengarajan, M. S. Zawadzki, and R. E. Hodges, "Design, analysis, and development of a large Ka-band slot array for digital beamforming application," *IEEE Trans. Antennas Propag.*, vol. 57, no. 10, pp. 3103–3109, Oct. 2009.

[7] C. E. Miller et al., "The ABoVE L-band and P-band airborne synthetic aperture radar surveys," *Earth Syst. Sci. Data*, vol. 16, no. 6, pp. 2605–2624, Jun. 2024.

[8] G. El-Arnauti, O. Saalmann, and A. R. Brenner, "Ultra-high resolution airborne experiments with a new Ka-band SAR sensor," in *Proc. Eur. Radar Conf. (EURAD)*, Nuermberg, Germany, Oct. 2017, pp. 409–412.

[9] R. Horn, A. Nottensteiner, A. Reigber, J. Fischer, and R. Scheiber, "F-SAR—DLR's new multifrequency polarimetric airborne SAR," in *Proc. IEEE Int. Geosci. Remote Sens. Symp.*, Cape Town, South Africa, Jul. 2009, pp. 902–905.

[10] M. Limbach, A. D. Maria, A. Kosc, M. Jaeger, and R. Horn, "DLR–F-SAR P-band antenna–design, measurements and results," in *Proc. 11th Eur. Conf. Synth. Aperture Radar (EUSAR)*, Hamburg, Germany, Jun. 2016, pp. 1–5.

[11] D. Lorente, M. Limbach, B. Gabler, H. Esteban, and V. E. Boria, "Highly integrated low-profile multilayer dual-polarized phased array antenna with truncated cavities for first pulsed bistatic L-band airborne SAR sensor," *IEEE Access*, vol. 12, pp. 435–449, 2024.

[12] M. Limbach, A. Di Maria, A. Reigber, B. Gabler, R. Horn, and A. Kosc, "S-band antenna for airborne polarimetric and interferometric SAR-applications," in *Proc. 7th Eur. Conf. Antennas Propag. (EuCAP)*, Gothenburg, Sweden, Apr. 2013, pp. 2968–2972.

[13] A. Di Maria, M. Limbach, R. Horn, and A. Reigber, "Design and measurements of a C-band array for high power high bandwidth SAR application," in *Proc. 7th Eur. Conf. Antennas Propag. (EuCAP)*, Gothenburg, Sweden, Apr. 2013, pp. 1803–1806.

[14] J. V. Fayne, L. C. Smith, L. H. Pitcher, E. D. Kyzivat, S. W. Cooley, M. G. Cooper, M. W. Denbina, A. C. Chen, C. W. Chen, and T. M. Pavelsky, "Airborne observations of arctic-boreal water surface elevations from AirSWOT Ka-band InSAR and LVIS LiDAR," *Environ. Res. Lett.*, vol. 15, no. 10, Oct. 2020, Art. no. 105005.

[15] J. Nouvel, H. Jeuland, G. Bonin, S. Roques, O. D. Plessis, and J. Peyret, "A Ka band imaging radar: DRIVE on board ONERA motorglider," in *Proc. IEEE Int. Symp. Geosci. Remote Sens.*, Denver, CO, USA, Jul. 2006, pp. 1–8.

[16] K. Tomiyasu, "Tutorial review of synthetic-aperture radar (SAR) with applications to imaging of the ocean surface," *Proc. IEEE*, vol. 66, no. 5, pp. 563–583, May 1978.

[17] R. C. Johnson, "Slot-antenna arrays," in *Antenna Engineering Handbook*, 3rd ed., New York, NY, USA: McGraw-Hill, 1993, pp. 1–39.

[18] L. Josefsson and S. R. Rengarajan, *Slotted Waveguide Array Antennas: Theory, Analysis and Design*. Rijeka, Croatia: SciTech, 2018.

[19] C. Roemer, "Slotted waveguide structures in phased array antennas," Ph.D. dissertation, Fac. Elect. Eng. Inf. Technol., Inst. Radio Freq. Eng. Electron. (IHE), Univ. Karlsruhe, Karlsruhe, Germany, 2008.

[20] H. S. Farahani, B. Rezaee, W. Boesch, and H. Paulitsch, "Ka-band slotted SIW phased array antenna," in *Proc. Int. Workshop Antennas Techn. (iWAT)*, Bukarest, Romania, Feb. 2020, pp. 1–4.

[21] D.-Y. Kim, W. Chung, C. Park, S. Lee, and S. Nam, "Design of a 45°-inclined SIW resonant series slot array antenna for *Ka* -band," *IEEE Antennas Wireless Propag. Lett.*, vol. 10, pp. 318–321, 2011.

[22] A. Ünal and O. Dinçer, "Ka band substrate integrated waveguide slot array antenna with high efficiency," in *Proc. IEEE Int. Symp. Antennas Propag. USNC/URSI Nat. Radio Sci. Meeting*, Vancouver, BC, Canada, Jul. 2015, pp. 484–485.

[23] T. Ding, M. Wang, J. Guo, J. Xiao, and Q. Ye, "Ka-band SIW slot antenna array with low sidelobe level," in *Proc. Int. Conf. Microw. Millim. Wave Technol. (ICMMT)*, Nanjing, China, May 2021, pp. 1–3.

[24] N. Sielck, T. Schwiers, K. Erkelenz, A. Koelpin, and A. F. Jacob, "Self-diplexing, dual-polarized Ka-band SIW slot antenna with integrated K-band patch," in *Proc. 14th German Microw. Conf. (GeMiC)*, Ulm, Germany, May 2022, pp. 172–175.

[25] D. Kim, Y. Lim, and S. Nam, "Design of a Ka-band dual polarized SIW slot array antenna with low mutual coupling," in *Proc. 7th Global Symp. Millim. Waves (GSMM)*, Seoul, South Korea, May 2014, pp. 21–23.

[26] D. Kim, S. Yun, W. Chung, S. Lee, and S. Nam, "Dual and linearly polarized SIW series slot array antenna for Ka band," in *Proc. Int. Symp. Antennas Propag. (ISAP)*, Jeja, South Korea, Oct. 2011, pp. 1–4.

[27] R. K. Enjiu and M. B. Perotoni, "Slotted waveguide antenna design using 3D EM simulation," *Microwave J.*, vol. 56, no. 7, pp. 72–84, Aug. 2013.

[28] J. Hirokawa, K. Sakurai, M. Ando, and N. Goto, "An analysis of waveguide T junction with an inductive post," *IEEE Trans. Microw. Theory Techn.*, vol. 39, no. 3, pp. 563–566, Mar. 1991.

[29] J. Uher, J. Bornemann, and U. Rosenberg, "Power dividers and combiners," in *Waveguide Components for Antenna Feed Systems: Theory and CAD*. Norwood, MA, USA: Artech House, 1993, pp. 343–355.

[30] S. Hashemi-Yeganeh and R. S. Elliott, "Analysis of untilted edge slots excited by tilted wires," *IEEE Trans. Antennas Propag.*, vol. 38, no. 11, pp. 1737–1745, Nov. 1990.

[31] J. Hirokawa and P.-S. Kildal, "Excitation of an untilted narrow-wall slot in a rectangular waveguide by using etched strips on a dielectric plate," *IEEE Trans. Antennas Propag.*, vol. 45, no. 6, pp. 1032–1037, Jun. 1997.

[32] J. J. W. Wang, "An untilted edge-slotted waveguide antenna array design," in *Proc. 3rd Int. Conf. Comput. Electromagn. Appl. (ICCEA)*, Nov. 1990, vol. 38, no. 11, pp. 208–211.

[33] D. Dudley, "An iris-excited slot radiator in the narrow wall of rectangular waveguide," *IRE Trans. Antennas Propag.*, vol. 9, no. 4, pp. 361–364, Jul. 1961.

[34] D. Dogan and Ö. A. Civi, "Edge wall slotted waveguide antenna with low cross polarization," in *Proc. IEEE Antennas Propag. Soc. Int. Symp.*, Toronto, ON, Canada, Jul. 2010, pp. 1–4.

[35] T. Zwick, *Antennen Und Mehrantennensysteme*. Karlsruhe, Germany: Karlsruhe Institute of Technology (KIT), 2021, p. 92.

[36] M. Moghavvemi, A. Mahabadi, and A. Farhang, "Multi-hole waveguide directional couplers," Munich Personal RePEc Arch. (MPRA), Munich, Germany, Tech. Rep. 46048, 2012. [Online]. Available: https://mpra.ub.uni-muenchen.de/46048/

[37] E. L. Ginzton and P. S. Goodwin, "A note on coaxial Bethe-hole directional couplers," *Proc. IRE*, vol. 38, no. 3, pp. 305–309, Mar. 1950.

[38] R. A. Bhatti, B.-Y. Park, Y.-T. Im, and S.-O. Park, "Design of a planar slotted waveguide array antenna for X-band radar applications," *J. Electromagn. Eng. Sci.*, vol. 11, no. 2, pp. 97–104, Jun. 2011.

[39] H. M. E. Misilmani, M. Al-Husseini, K. Y. Kabalan, and A. El-Hajj, "A design procedure for slotted waveguide antennas with specified sidelobe levels," in *Proc. Int. Conf. High Perform. Comput. Simulation (HPCS)*, Bologna, Italy, Jul. 2014, pp. 828–832.

[40] R. Kumar, P. K. Verma, and M. Singh, "Slotted waveguide array antenna with compact feed network at Ka-band band," in *Proc. Asia–Pacific Microw. Conf. (APMC)*, New Delhi, India, Dec. 2016, pp. 1–4.

[41] E. Schreiber, "Entwicklung und Aufbau einer breitbandigen Hohlleiterschlitzantenne für radiometrische Anwendungen," M.S. thesis, Fac. Elect. Eng. Inf. Technol., Inst. Radio Freq. Eng. Electron. (IHE), Univ. Karlsruhe, Karlsruhe, Germany, 2008.

[42] B. Li, L. Li, and C.-H. Liang, "The rectangular waveguide board wall slot array antenna with EBG structure," *J. Electromagn. Waves Appl.*, vol. 19, no. 13, pp. 1807–1815, Jan. 2005.
[43] A. M. Khan, M. M. Ahmed, U. Rafique, and S. Khan, "Design, analysis and fabrication of an inside-grooved slotted waveguide array antenna for HPM applications," *IEEE Access*, vol. 11, pp. 50116–50129, 2023.
[44] M. Limbach, B. Gabler, R. Horn, and A. Reigber, "DLR-HR compact test range facility," in *Proc. 3rd Eur. Conf. Antennas Propag.*, Mar. 2009, pp. 2186–2189.
[45] Y. Cong and W. Dou, "Design of dual-polarized waveguide slotted antenna array for Ka-band application," in *Proc. 9th Int. Symp. Antennas, Propag. EM Theory*, Guangzhou, China, Nov. 2010, pp. 97–100.
[46] M. Ferrando-Rocher, J. I. Herranz-Herruzo, A. Valero-Nogueira, B. Bernando-Clemente, A. U. Zaman, and J. Yang, "8×8 Ka-band dual-polarized array antenna based on gap waveguide technology," *IEEE Trans. Antennas Propag.*, vol. 67, no. 7, pp. 4579–4588, Jul. 2019.
[47] T. Li, H. Meng, and W. Dou, "Design and implementation of dual-frequency dual-polarization slotted waveguide antenna array for Ka-band application," *IEEE Antennas Wireless Propag. Lett.*, vol. 13, pp. 1317–1320, 2014.
[48] T. Li and W. Dou, "Design of an edge slotted waveguide antenna array based on T-shaped cross-section waveguide," *Int. J. Antennas Propag.*, vol. 2017, no. 1, 2017, Art. no. 7385357.
[49] L. F. Herrán, A. A. Brazalez, and E. Rajo-Iglesias, "Ka-band planar slotted waveguide array based on groove gap waveguide technology with a glide-symmetric holey metasurface," *Sci. Rep.*, vol. 11, no. 1, Apr. 2021, Art. no. 8697.
[50] C. Zhao, X. Li, C. Sun, H. Huang, and Y. Liu, "Design of a low-SLL SIW slot array antenna with a large declination in *Ka* -band," *IEEE Access*, vol. 7, pp. 120541–120547, 2019.
[51] S. Ye, J. Hu, L. Li, Y. Ma, and K. Qin, "High gain planar antenna array for Ka band SAR applications," in *Proc. China Int. SAR Symp. (CISS)*, Shanghai, China, Oct. 2018, pp. 1–3.
[52] J. F. Nouvel, P. Dubois-Fernandez, and X. Dupuis, "The KaSAR airborne campaign," in *Proc. IEEE Int. Geosci. Remote Sens. Symp. (IGARSS)*, Melbourne, VIC, Australia, Jan. 2013, pp. 4471–4474.

ALICJA SCHREIBER was born in Kętrzyn, Poland, in 1984. She received the double degree in electronic and telecommunication from Karlsruhe Institute of Technology (KIT), Germany, and Gdańsk University of Technology, Poland, in 2010.

She is currently a Research Scientist with the Antenna Group, Microwaves and Radar Institute, German Aerospace Center (DLR), Oberpfaffenhofen, Germany. Her research interest includes antenna design and simulation in different frequency bands for airborne synthetic aperture radar systems.

MARKUS LIMBACH is currently a Senior Research Associate and the Head of the Antenna Group, Microwaves and Radar Institute, German Aerospace Center (DLR), Oberpfaffenhofen, Germany. His research interests include antenna design and simulation for airborne synthetic aperture radar applications.

BERND GABLER (Member, IEEE) received the degree in telecommunication engineering from Munich University of Applied Sciences, Germany, in 1990.

He is currently a Senior Research Associate and the Head of the Compact Antenna Test Range, Microwaves and Radar Institute, German Aerospace Center (DLR), Oberpfaffenhofen, Germany. His research interest includes antenna and radar cross-section measurement techniques and analysis.